Research and Development Technical Report

ECOM-4498

TEMPERATURE COMPENSATED CRYSTAL OSCILLATOR (TCXO) DESIGN AIDS: FREQUENCY-TEMPERATURE RESONATOR CHARACTERISTICS AS SHIFTED BY SERIES CAPACITORS

Arthur Ballato

Electronics Technology & Devices Laboratory

May 1977

ECOM

US ARMY ELECTRONICS COMMAND FORT MONMOUTH, NEW JERSEY 07703

NOTICES

Disclaimers

The findings in this report are not to be construed as an official Department of the Army position, unless so designated by other authorized documents.

The citation of trade names and names of manufacturers in this report is not to be construed as official Government indorsement or approval of commercial products or services referenced herein.

Disposition

Destroy this report when it is no longer needed. Do not return it to the originator.

UNCLASSIFIED

SECURITY CLASSIFICATION OF THIS PAGE *(When Data Entered)*

REPORT DOCUMENTATION PAGE

READ INSTRUCTIONS BEFORE COMPLETING FORM

1. REPORT NUMBER: ECOM-4189	2. GOVT ACCESSION NO.
3. RECIPIENT'S CATALOG NUMBER	
4. TITLE *(and Subtitle)*: TEMPERATURE COMPENSATED CRYSTAL OSCILLATOR (TCXO) DESIGN AIDS: FREQUENCY-TEMPERATURE RESONATOR CHARACTERISTICS AS SHIFTED BY SERIES CAPACITORS.	5. TYPE OF REPORT & PERIOD COVERED: Technical Report, April 77
	6. PERFORMING ORG. REPORT NUMBER
7. AUTHOR(s): Arthur Ballato	8. CONTRACT OR GRANT NUMBER(s)
9. PERFORMING ORGANIZATION NAME AND ADDRESS: US Army Electronics Command, ATTN: DRSEL-TL-ML, Fort Monmouth, NJ 07703	10. PROGRAM ELEMENT, PROJECT, TASK AREA & WORK UNIT NUMBERS: 1T1 61101 A 91A 09 455
11. CONTROLLING OFFICE NAME AND ADDRESS: US Army Electronics Command, ATTN: DRSEL-TL-ML, Fort Monmouth, NJ 07703	12. REPORT DATE: May 1977
	13. NUMBER OF PAGES: 59
14. MONITORING AGENCY NAME & ADDRESS *(if different from Controlling Office)*	15. SECURITY CLASS. *(of this report)*: UNCLASSIFIED
	15a. DECLASSIFICATION/DOWNGRADING SCHEDULE

16. DISTRIBUTION STATEMENT *(of this Report)*

Statement A.
Approved for public release; distribution unlimited.

17. DISTRIBUTION STATEMENT *(of the abstract entered in Block 20, if different from Report)*

18. SUPPLEMENTARY NOTES

19. KEY WORDS *(Continue on reverse side if necessary and identify by block number)*

Quartz oscillators	Frequency stability	Temperature compensation
Quartz vibrators	Frequency control	AT-cut resonators
Crystal oscillators	Piezoelectric vibrators	SC-cut resonators
Crystal resonators	Piezoelectric crystals	Temperature compensated crystal oscillators (TCXO's)

20. ABSTRACT *(Continue on reverse side if necessary and identify by block number)*

Resonators for TCXO application are required to have accurately-characterized frequency-temperature (f-T) curves and equivalent network parameters. This report describes how the circuit parameters, critical resonator frequencies, and temperature coefficients depend on material constants of the crystal and geometrical factors. These constants are tabulated for AT- and SC-cut quartz. It further explains the observed f-T curve shift between resonator operation with and without series load capacitors. Simple relations are given for treating this effect, along with charts and other design aids. These are used in a

DD FORM 1 JAN 73 1473 EDITION OF 1 NOV 65 IS OBSOLETE

UNCLASSIFIED

SECURITY CLASSIFICATION OF THIS PAGE *(When Data Entered)*

20. ABSTRACT (continued)

practical example involving an AT-cut resonator for a typical TCXO application.

CONTENTS

INTRODUCTION

One of the important developments in high precision frequency control is the temperature-compensated crystal oscillator (TCXO).[1-25] This device incorporates a temperature sensor and associated circuitry to derive a correction signal that is used to stabilize the oscillator. The most frequently used method for producing the correction consists of adjustment of a varactor in series with the crystal resonator controlling the oscillator. In the design of the compensation network, it is necessary to know the frequency-temperature (f-T) characteristic of the crystal to be compensated, but this alone is not sufficient. It is found experimentally that the effective f-T curve is altered upon insertion in the uncompensated oscillator.

This report explains the reason for this behavior, gives simple formulas for calculating the size of the effect, and provides design aids in the form of curves, with an example drawn from current practice.

FREQUENCY EQUATIONS

Virtually all current TCXO applications employ thickness mode quartz vibrators. For this class of vibrator, excited by an electric field in the thickness direction, the input admittance, assuming no loss and a single driven mode, is[26]

$$Y = j\omega C_o/(1 - k^2 \tan X/X). \tag{1}$$

In (1),

$$C_o = \varepsilon A/2h, \tag{2}$$

where C_o is the vibrator static capacitance, ε is the effective permittivity, A is the electrode area, and 2h is the thickness. The quantity k is the piezoelectric coupling factor, while X is defined as

$$X = (\pi/2)(f/f_{Ao}^{(1)}), \tag{3}$$

with f the frequency variable (= $\omega/2\pi$), and $f_{Ao}^{(1)}$ the antiresonance frequency at the fundamental harmonic (M = 1), in the absence of mass-loading.

Antiresonance

The antiresonance frequencies are sometimes referred to as the mechanical resonances, these being the frequencies for which an open-circuited resonator is one-half times an integer wavelength in thickness. If the crystal vibrator plate is of density ρ, and the mode under consideration has elastic constant $\bar{c}$ (piezoelectrically stiffened), then the acoustic velocity is

$$v = (\bar{c}/\rho)^{1/2}, \tag{4}$$

and the antiresonance frequencies are

$$f_{Ao}^{(M)} = M\,(\bar{c}/\rho)^{1/2}/4h \tag{5}$$

The harmonics of (5) are integrally-related in the absence of mass-loading (negligible electrode coatings); each harmonic corresponds to a pole of the tangent function in (1).

Resonance

Setting the denominator of (1) equal to zero yields the normalized resonance frequencies as roots of the equation

$$\tan X = X/k^2. \tag{6}$$

The roots of (6), denoted $X_{Ro}^{(M)}$, are not harmonically related; the resonance frequencies are obtained from the $X_{Ro}^{(M)}$ by means of (3):

$$X_{Ro}^{(M)} = (\pi/2)(f_{Ro}^{(M)}/f_{Ao}^{(1)}). \tag{7}$$

Figure 1 displays graphical solutions to (6), from which is seen how the resonance-antiresonance frequency difference $|f_{Ro}^{(M)} - f_{Ao}^{(M)}|$ decreases with increasing M, and also how the difference, at any M, is affected by changes in the piezoelectric coupling factor k.

A plot of $X_{Ro}^{(M)}$ versus k for M = 1, 3, and 5 is given in Figure 2.[27] An alternative representation, and one that is better suited from the standpoint of graphical accuracy, is that of frequency displacement[28,29,30]

$$\delta_{Ro}^{(M)} = M - (2X_{Ro}^{(M)}/\pi) = M - \Omega_{Ro}^{(M)}. \tag{8}$$

Frequency displacement appears in a natural manner when the topic of approximations is taken up in a later section. It is clear that the antiresonance displacement in the absence of mass-loading, $\delta_{Ao}^{(M)}$, vanishes identically by virtue of (3), (5), and (8), written with the appropriate subscripts. Figure 3 shows the variation of $\delta_{Ro}^{(M)}$ with k and M, obtained from (6) and (8).

Load

Insertion of a load capacitor C_L in series with the vibrator modifies (1), but the entire effect may be subsumed into changes in the values of C_o and k^2. Denoting the effective values of C_o and k^2 in the presence of C_L as C_{oL} and k_L^2, respectively, and defining the quantity α as[31]

$$\alpha = C_o/(C_o + C_L), \tag{9}$$

the effective values become

$$C_{oL} = C_o\ (1 - \alpha), \tag{10}$$

$$k_L^2 = k^2\ (1 - \alpha). \tag{11}$$

Using k_L^2 in (6) yields the load frequencies $X_{Lo}^{(M)}$, $f_{Lo}^{(M)}$, and $\delta_{Lo}^{(M)}$ in place of the corresponding resonance quantities. In the limit $\alpha \to 1$ ($C_L \to o$), the load frequencies approach the antiresonance frequencies, while the limit $\alpha \to o$ ($C_L \to \infty$) reduces the frequencies to the resonances.

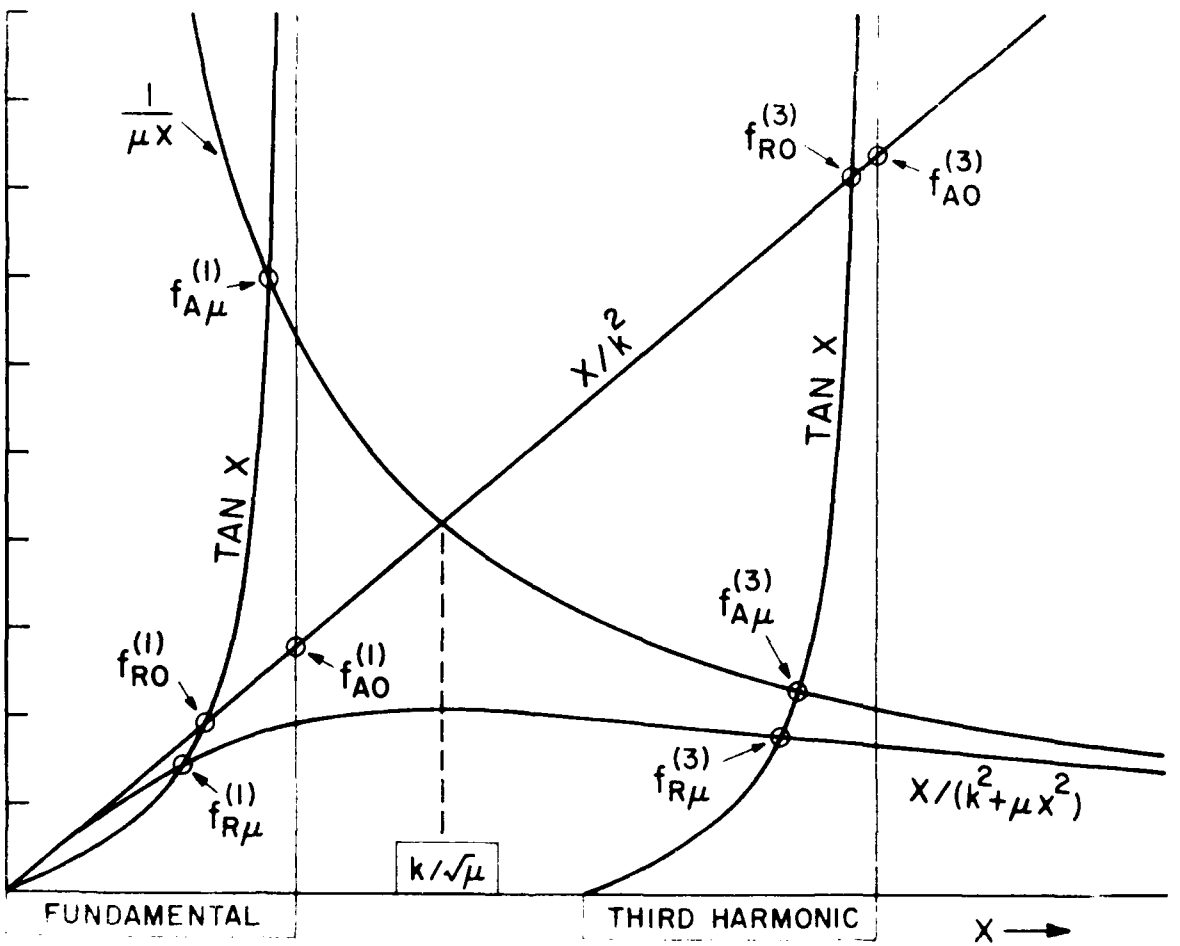

FIG. 2. GRAPHICAL FREQUENCY CONSTRUCTION.

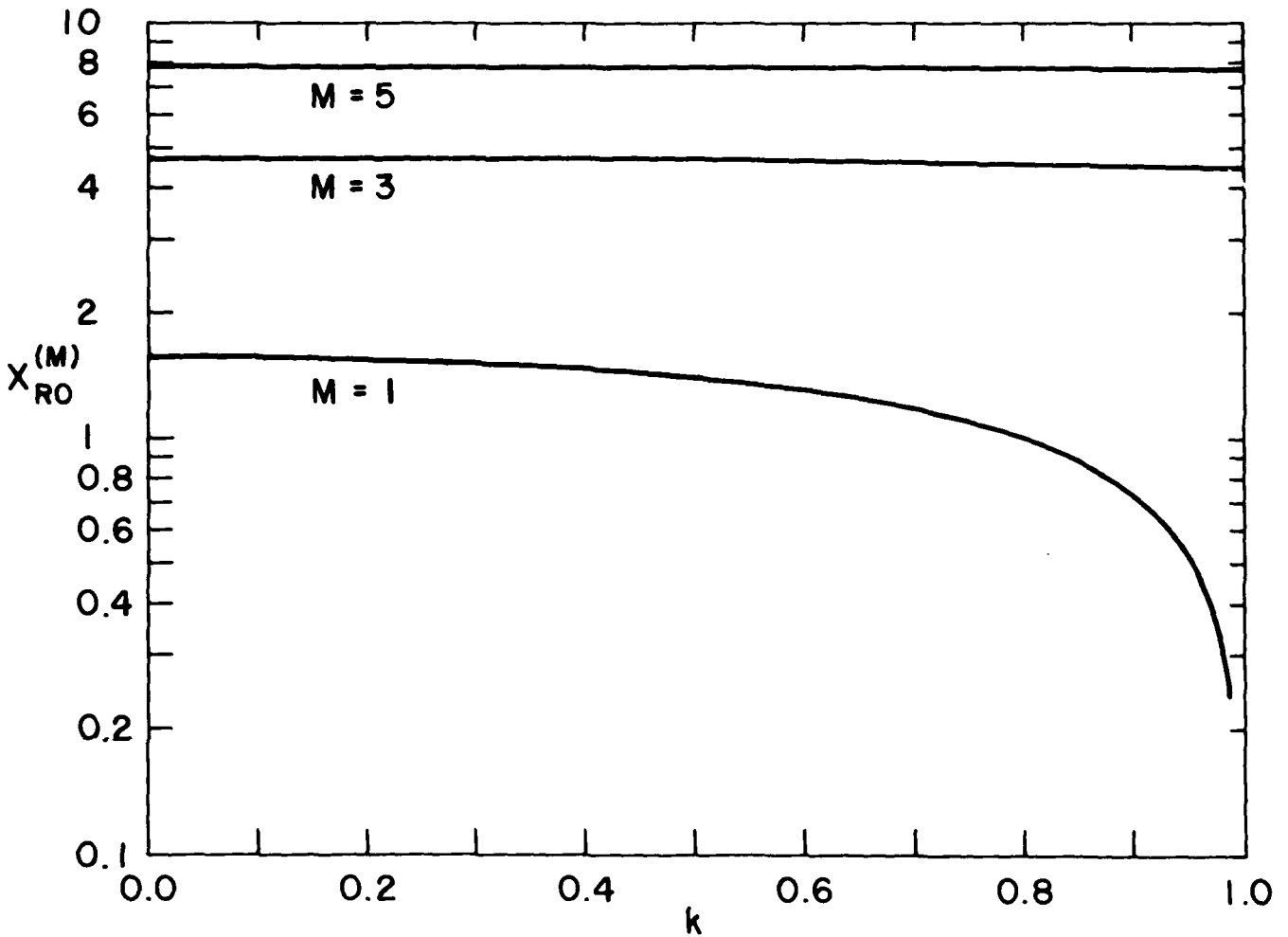

FIGURE 2. NORMALIZED FREQUENCY VERSUS COUPLING.

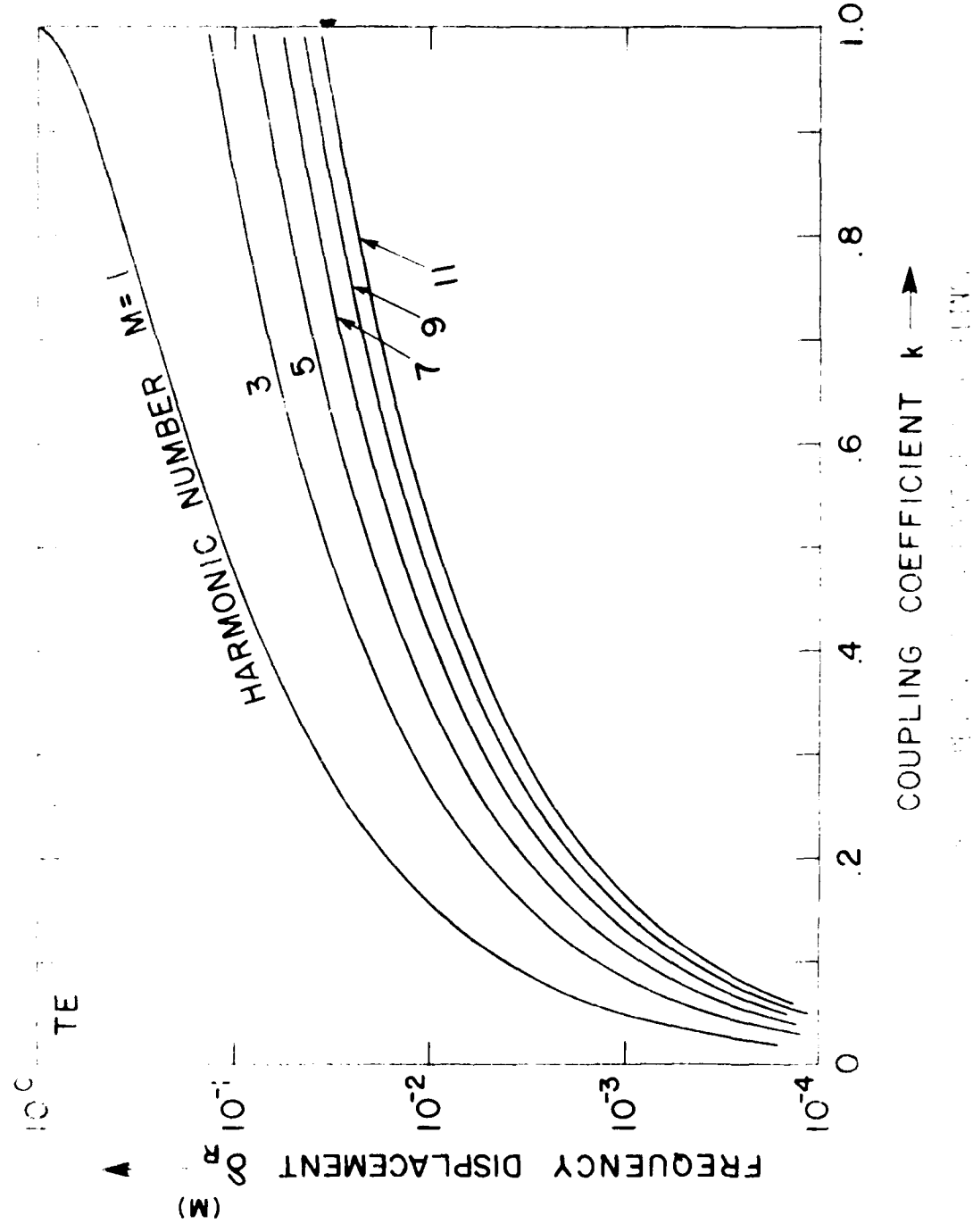
FREQUENCY DISPLACEMENT δ_R (M)
10^{-1}
10^{-2}
10^{-3}
10^{-4}
0
.2
.4
.6
.8
1.0
COUPLING COEFFICIENT k
HARMONIC NUMBER M= 1
3
5
7 9 11
TE

The inclusion of loss is easily dealt with; if the loss is considered to arise from a material viscosity η, then substitution of[32]

$$\hat{X} = X(1 - j\omega\eta/2\bar{c}) \tag{12}$$

for X in the foregoing describes the loss accurately. Table 1 gives a list of pertinent material constants for two selected cuts of quartz. The AT-cut is at present the most popular quartz cut for thickness mode plates. The newly-introduced SC-cut is a doubly rotated cut[32-35] that is expected to play an increasing role in TCXO applications, particularly for fast-warmup operation, because of its superior cancellation of certain nonlinear elastic effects.

TABLE 1. PHYSICAL AND ELECTRICAL PARAMETERS ASSOCIATED WITH AT- AND SC-CUT QUARTZ RESONATORS: NUMERICAL VALUES.

		AT-cut		SC-cut	
		Orientation (YX$\omega\ell$)Φ/θ			
Quantity	Unit	Φ = 0°	θ = +35.25°	Φ = 21.93°	θ = +33.93°
ρ	10^{+3} kg/m^3	2.649		2.649	
ε	pF/m	39.82		39.78	
e	10^{-2} C/m	9.49		5.82	
$\bar{c}$	10^{+9} Pa	29.24		34.23	
η	10^{-4} Pa · s	3.46		4.02	
N	MHz - mm	1.661		1.797	
$\partial N/\partial\theta$	kHz - mm/°θ	2.09		1.03	
$\partial N/\partial\Phi$	kHz - mm/°Φ	0		12.0	
$\lvert k\rvert$	%	8.80		4.99	
$\partial\lvert k\rvert/\partial\theta$	10^{-3}/°θ	-2.97		1.75	
$\partial\lvert k\rvert/\partial\Phi$	10^{-3}/°Φ	0		-2.78	
τ_1	fs	11.8		11.7	
r	---	159.4		495.8	
$\partial r/\partial\theta$	10^{+2}/°θ	0.11		-0.35	
$\partial r/\partial\Phi$	10^{+2}/°Φ	0		0.55	
Γ_1	fF/m	249.8		80.3	
ρ_1	10^{-3} Ω/m	47.2		146.	
ψ_1	---	0.60 -- 0.90		0.60 -- 0.90	

MASS-LOADING FREQUENCY EFFECTS

In normal practice the electrode coatings depress the frequency spectrum non-negligibly. For coatings of mass $\bar{m}$ per unit area lumped on each surface, the reduced mass-loading variable is

$$\mu = \bar{m}/\rho h. \tag{13}$$

With the inclusion of μ (1) is replaced by

$$Y = j\omega C_o/[\ 1 - (\frac{k^2}{1 - \mu X \tan X}) \cdot \frac{\tan X}{X}\ ]. \tag{14}$$

Antiresonance

The zeros of (14) lead to the equation determining the antiresonances:

$$\mu X \tan X = 1; \tag{15}$$

the roots, $X_{A\mu}^{(M)}$, of (15) are no longer harmonically-related. From the $X_{A\mu}^{(M)}$ the frequencies $f_{A\mu}^{(M)}$ are determined using

$$X_{A\mu}^{(M)} = (\pi/2)\ (f_{A\mu}^{(M)}/f_{Ao}^{(1)}), \tag{16}$$

and the displacements $\delta_{A\mu}^{(M)}$ follow from the analog of (8):

$$\delta_{A\mu}^{(M)} = M - (2X_{A\mu}^{(M)}/\pi) = M - \Omega_{A\mu}^{(M)}. \tag{17}$$

Figure 1 gives the graphical construction for the $f_{A\mu}^{(M)}$, and Figure 4 shows the frequency spectrum for $\Omega_{A\mu}^{(M)}$ as function of μ. The displacements $\delta_{A\mu}^{(M)}$ are similarly shown as functions of μ in Figure 5 for the curves marked k = 0.

Resonance

The poles of (14) lead to the equation determining the resonance frequencies:

$$\tan X = X/(k^2 + \mu X^2). \tag{18}$$

The roots of (18), $X_{R\mu}^{(M)}$ determine the $f_{R\mu}^{(M)}$ and $\delta_{R\mu}^{(M)}$ as follows:

$$X_{R\mu}^{(M)} = (\pi/2)(f_{R\mu}^{(M)}/f_{Ao}^{(1)}), \tag{19}$$

$$\delta_{R\mu}^{(M)} = M - (2X_{R\mu}^{(M)}/\pi) = M - \Omega_{R\mu}^{(M)}. \tag{20}$$

The graphical construction for $f_{R\mu}^{(M)}$ is also given in Figure 1. Figure 4 shows $\Omega_{R\mu}^{(M)}$ as function of μ. The quantity $\hat{\Omega}$ appearing on this figure is defined by

$$\hat{\Omega} = (2/\pi)(k/\sqrt{\mu}), \tag{21}$$

and gives a measure of the relative importance of μ and k in (18), as may be seen from Figure 1. In Figure 5 are found the solutions to (18), expressed

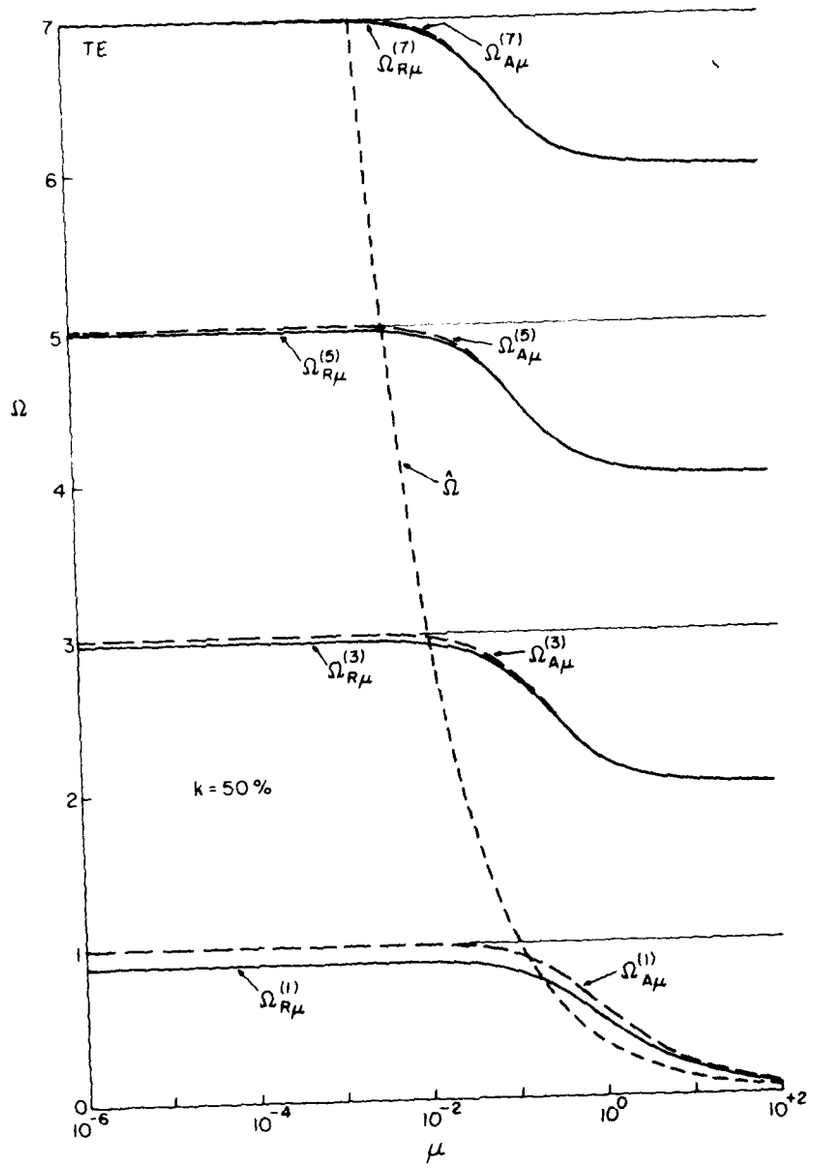

FIGURE 4. FREQUENCY SPECTRUM VERSUS MASS-LOADING.

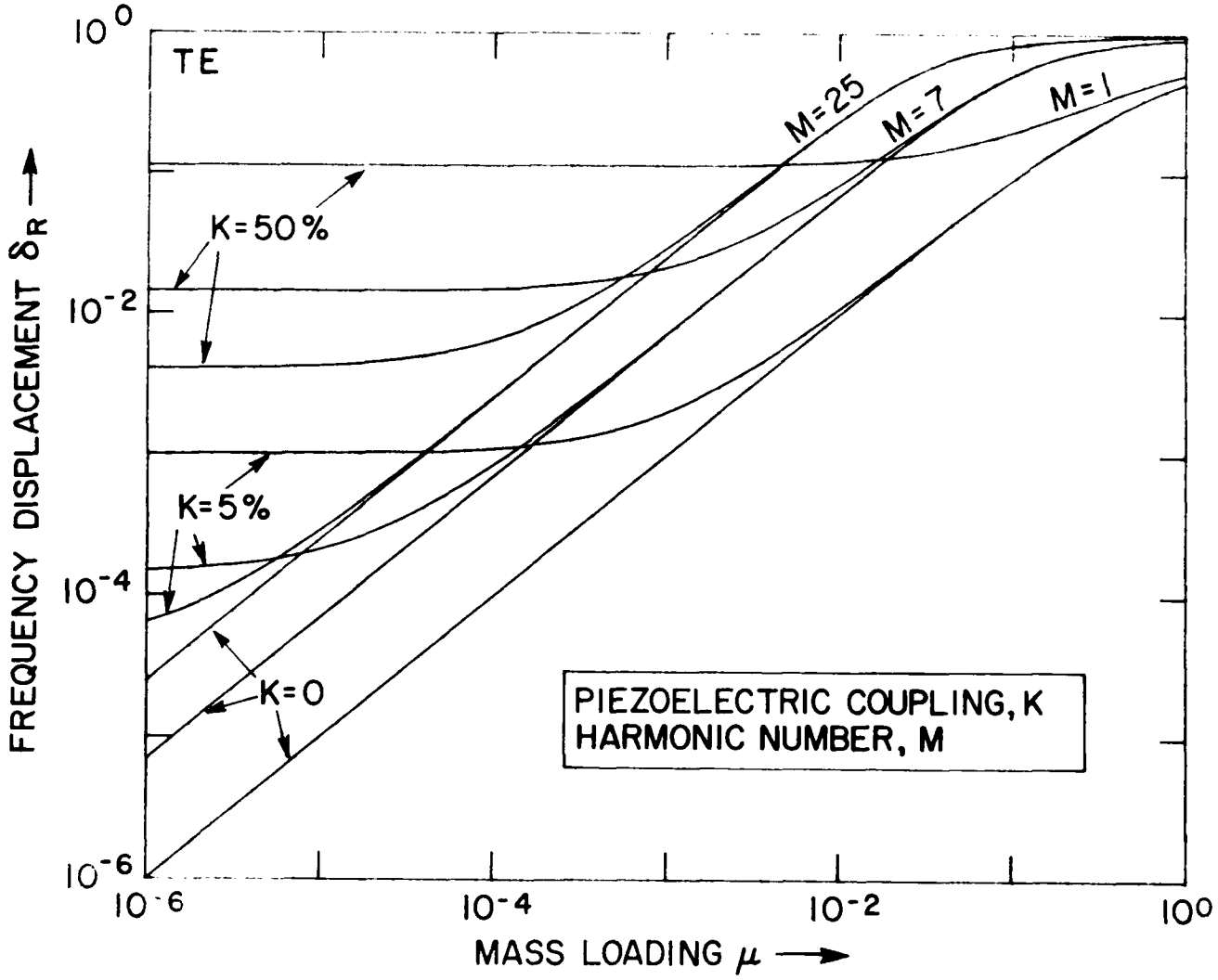

FIGURE 3. FREQUENCY DISPLACEMENT VERSUS MASS LOADING.

as displacements, plotted against μ for various k and M values. Figure 6 is a plot of $\delta_{R\mu}^{(1)}$ versus k for various μ values; Figure 7 is the companion graph of $\delta_{R\mu}^{(3)}$. A comparison of Figure 6 and Figure 7 indicates that as M increases, less μ is required to reach a given δ value.

Load

With C_L added in series to the mass-loaded vibrator, the quantities $X_{L\mu}^{(M)}$, $f_{L\mu}^{(M)}$, and $\delta_{L\mu}^{(M)}$ are defined in an obvious way. Equation (15) is unaffected, while k^2 in (18) is replaced by k_L^2 from (11) to yield the load frequencies and displacements. Figures 6 and 7 give the $\delta_{L\mu}^{(M)}$ when k_L is substituted for k.

CRITICAL FREQUENCY APPROXIMATIONS

Simple, approximate relations, usually adequate in practice, can be obtained from the transcendental relations (6), (15), and (18). The first approximation to $X_{Ro}^{(M)}$, valid for large M, and for smaller M when $k \ll 1$, is

$$X_{Ro}^{(M)} \simeq X_{Ao}^{(M)} \simeq (\pi/2)\ M; \tag{22}$$

the second approximation for $X_{Ro}^{(M)}$ is

$$X_{Ro}^{(M)} \simeq (\pi/2)M\ [\ 1 - (\frac{2k}{\pi M})^2\ ]. \tag{23}$$

The term $(2k/\pi M)^2$ was introduced by Bechmann,[36,37] and referred to by Cady[38] as "Bechmann's γ." With the inclusion of μ, (23) becomes

$$X_{R\mu}^{(M)} \simeq (\pi/2)\ M\ [\ (1 - \mu) - (\frac{2k}{\pi M})^2\ ], \tag{24}$$

while $X_{A\mu}^{(M)}$ is obtained from (24) by setting $k = 0$.

The approximations involving δ are found by using (17) in (15) and (20) in (18), simplifying, then expanding the tangent functions and truncating the result. One first arrives at[39]

$$\tan\ (\delta_{A\mu}^{(M)}\ \pi/2) = \mu\ (M - \delta_{A\mu}^{(M)})\ \pi/2, \tag{25}$$

and

$$\tan\ (\delta_{R\mu}^{(M)}\ \pi/2) = \mu\ (M - \delta_{R\mu}^{(M)})\ \pi/2 + 2k^2/\pi\ (M - \delta_{R\mu}^{(M)}), \tag{26}$$

with the equation for $\delta_{Ro}^{(M)}$ formed from (26) by setting $\mu = 0$. After suitable approximations are made, as indicated above, one gets

$$\delta_{Ro}^{(M)} \simeq M \cdot (\frac{2k}{\pi M})^2\ (1 + (\frac{2k}{\pi M})^2)^{-1} \simeq M \cdot (\frac{2k}{\pi M})^2. \tag{27}$$

For $\delta_{R\mu}^{(M)}$ the result is

$$\delta_{R\mu}^{(M)} \simeq (\delta_{Ro}^{(M)} + M\mu)/(1 + M\mu); \tag{28}$$

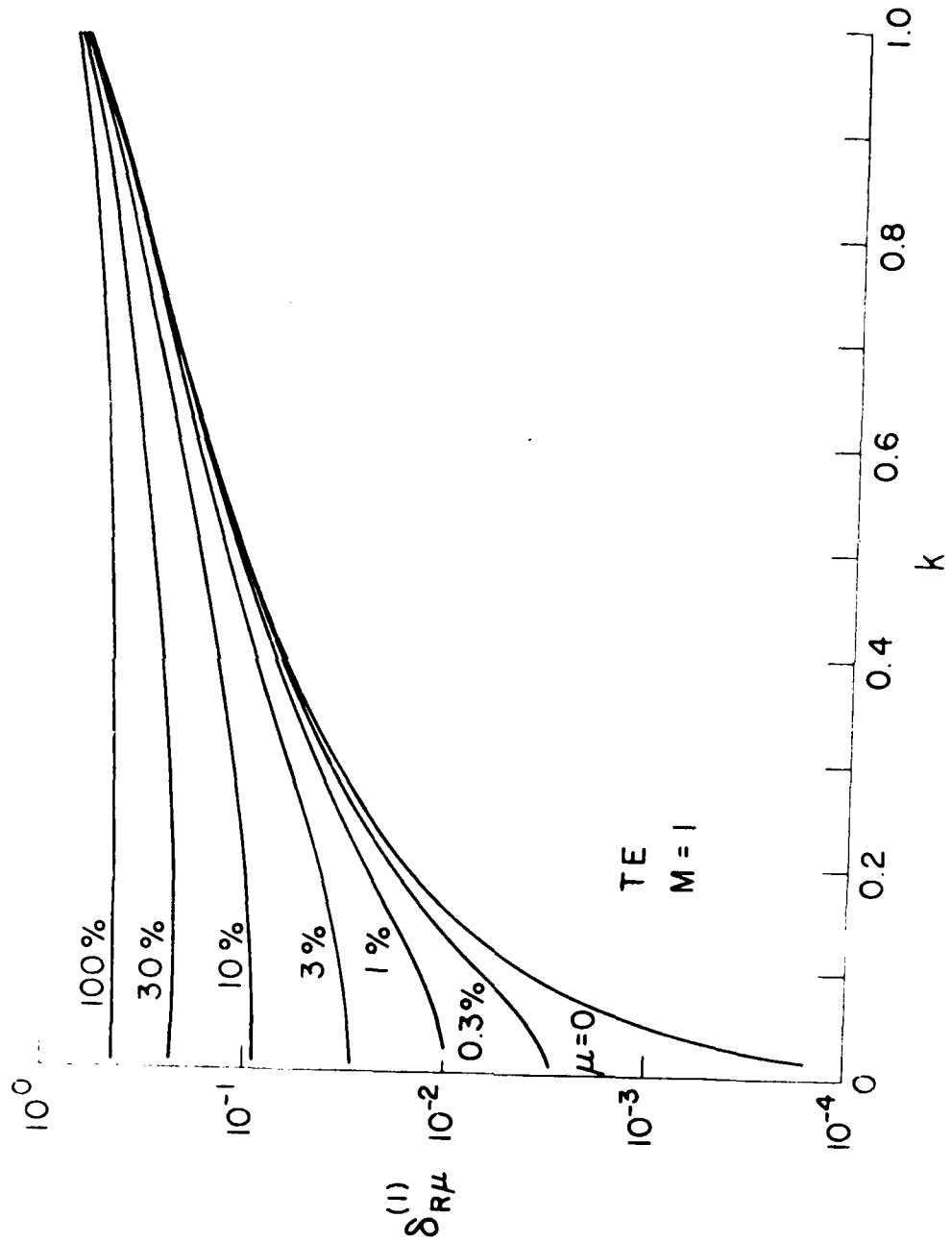
100%
30%
10%
3%
1%
0.3%
μ=0
TE
M = 1
10^{0}
10^{-1}
10^{-2}
10^{-3}
10^{-4}
$\delta^{(1)}_{R\mu}$
0
0.2
0.4
0.6
0.8
1.0
k

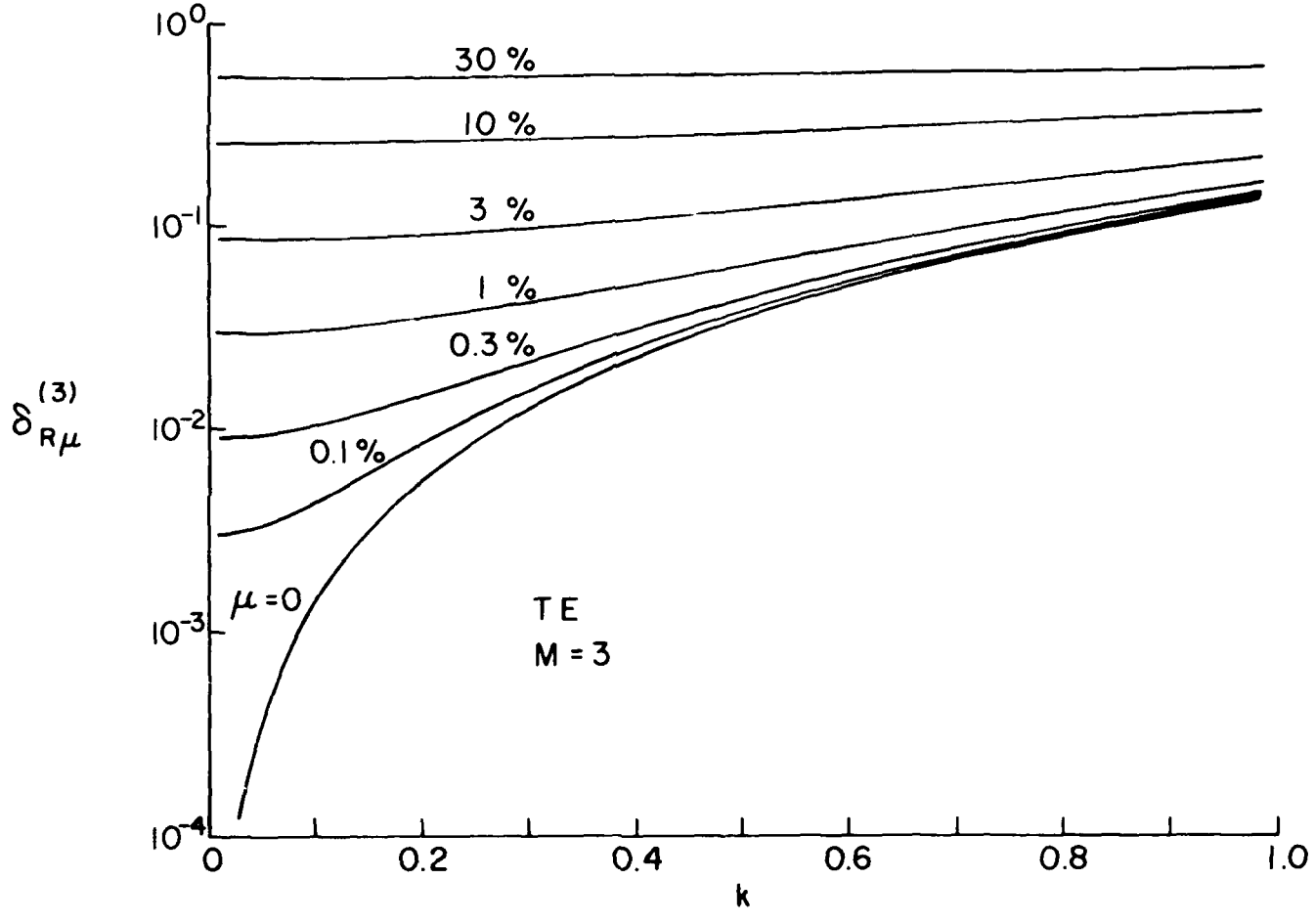

FIGURE 7. FREQUENCY DISPLACEMENT VERSUS COUPLING FOR M = 3.

for $\delta_{M\mu}^{(M)}$ one simply uses (28) with $\delta_{Ro}^{(M)}$ set to zero.

For some applications it is helpful to know the relationship between the resonance frequencies at two harmonics, normalized by the harmonic numbers. The approximate relation is found from (8) and (27) to be

$$(\Omega_{Ro}^{(M)}/M) - (\Omega_{Ro}^{(N)}/N) \approx (\frac{2k}{\pi})^2 \cdot (1/N^2 - 1/M^2). \qquad (29)$$

Introduction of a load capacitor leads to a frequency displacement of $\delta_{Lo}^{(M)}$, which is approximated by using (27), with k^2 replaced by k_L^2 as given by (11). One similarly finds $\delta_{L\mu}^{(M)}$ from (28) and (11).

In view of the dependencies of δ upon α and M, one may seek a relationship between harmonic and α such that the relation

$$\delta_{Ro}^{(M)} = \delta_{Lo}^{(N)} \qquad (30)$$

holds. The result is

$$\alpha = (M - N)/M, \qquad (31)$$

meaning that, as far as the frequency displacements are concerned, operation at harmonic N with α given by (31) is equivalent to operation at harmonic M without C_L.

FREQUENCY-TEMPERATURE BEHAVIOR

Resonators for TCXO application are required to have precisely known frequency-temperature characteristics so that the compensatory network can be properly designed. Bechmann[40] found that AT-cut resonators could be described adequately, even over a rather wide temperature range, by a three-term power series. If the frequency of interest is f_o at temperature T_o, then with $\Delta T = T - T_o$,

$$(f - f_o)/f_o = \Delta f/f_o = a_o \Delta T + b_o \Delta T^2 + c_o \Delta T^3,$$

gives the frequency at temperature T. Table 2 gives values for the quantities a_o, b_o, and c_o and their angle gradients for the AT- and SC-cuts. The coefficients a_o, b_o, and c_o vary with orientation angle, mass-loading, and value of series load capacitor with the zero subscripts denoting the values at zero μ and α, and at reference angles Φ_o, θ_o. The coefficient "a" is synonymous with T_{fR} appearing in the sequel.

Angular Dependence

The variation with angle is also treated by means of power series expansions, normally using only the constant and linear terms:[41]

$$q = q_o + (\partial q/\partial\theta) \cdot \Delta\theta + (\partial q/\partial\Phi) \cdot \Delta\Phi, \qquad (32)$$

where q is a, b, or c, and $\Delta\theta = \theta - \theta_o$, $\Delta\Phi = \Phi - \Phi_o$.

TABLE 2. THERMAL PARAMETERS ASSOCIATED WITH AT- AND SC-CUT QUARTZ RESONATORS: NUMERICAL VALUES.

		AT-cut		SC-cut	
		Orientation (YX$\omega\ell$)Φ/θ			
Quantity	Unit	Φ = 0°	θ = +35.25°	Φ = 21.93°	θ = +33.93°
a_o	$10^{-6}/K$	0		0	
b_o	$10^{-9}/K^2$	-0.45		-12.3	
c_o	$10^{-12}/K^3$	108.6		58.2	
$\partial a/\partial\theta$	$10^{-6}/K,{}^o\theta$	-5.08		-3.78	
$\partial b/\partial\theta$	$10^{-9}/K^2,{}^o\theta$	-4.7		1.6	
$\partial c/\partial\theta$	$10^{-12}/K^3,{}^o\theta$	-20.		-18.	
$\partial^2 a/\partial\theta^2$	$10^{-9}/K,({}^o\theta)^2$	0.96		---	
$\partial a/\partial\Phi$	$10^{-6}/K,{}^o\Phi$	0		-0.18	
$\partial b/\partial\Phi$	$10^{-9}/K^2,{}^o\Phi$	0		-1.6	
$\partial c/\partial\Phi$	$10^{-12}/K^3,{}^o\Phi$	0		-3.8	
$\partial^2 a/\partial\Phi^2$	$10^{-9}/K,({}^o\Phi)^2$	-18.0		---	
$\partial a/\partial\mu$	$10^{-6}/K,(\%\mu)$	-0.24		-0.23	
T_i	°C	26.4		95.4	
$\partial T_i/\partial\theta$	$K/{}^o\theta$	14.9		12.6	
$\partial T_i/\partial\Phi$	$K/{}^o\Phi$	0		13.8	
$\partial T_i/\partial\mu$	$K/(\%\mu)$	-5.45		---	
T_{Co}	$10^{-6}/K$	29.7		29.7	
T_ε	$10^{-6}/K$	31.8		31.8	
T_μ	$10^{-6}/K$	23.3		23.3	
T_x	$10^{-6}/K$	-0.245		-0.213	
$\alpha(X_1'')$	$10^{-6}/K$	13.7		13.7	
$\alpha(X_2'')$	$10^{-6}/K$	11.6		11.6	
$\alpha(X_3'')$	$10^{-6}/K$	9.56		9.56	
T_k	$10^{-6}/K$	88.2		224.	
$\partial T_k/\partial\theta$	$10^{-6}/K,{}^o\theta$	16.0		-9.60	
$\partial T_k/\partial\Phi$	$10^{-6}/K,{}^o\Phi$	0		17.5	
T_r	$10^{-6}/K$	-176.		-448.	

For the AT-cut, $\partial q/\partial\Phi \equiv 0$ due to crystal symmetry considerations, so the expansion in this case has to be carried out to second order:[42]

$$q = q_o + (\partial q/\partial\theta) \cdot \Delta\theta + \tfrac{1}{2}(\partial^2 q/\partial\Phi^2) \cdot \Phi^2. \qquad (34)$$

Figure 8 shows the frequency-temperature-angle characteristics for the AT-cut. The normalized frequency excursions, δf, between the maxima and minima in Figure 8 are shown in Figure 9 as function of angular difference, $\Delta\theta$, from the reference angle θ_o. This curve is very important because δf enters directly into most TCXO design procedures. In Table 3 are presented the first- , second- , and third-order temperature coefficients for the AT-cut of quartz as function of departure from the reference angle.

TABLE 3. TEMPERATURE COEFFICIENTS AND FREQUENCY EXCURSIONS FOR AT-CUT QUARTZ.

$\Delta\theta$	a	b	c	δf
Minutes	$10^{-6}/K$	$10^{-9}/K^2$	$10^{-12}/K^3$	10^{-6}
0	0	0.390	109.5	0
½	-0.043	0.351	109.3	0.65
1	-0.086	0.312	109.2	1.85
1½	-0.129	0.273	109.0	3.40
2	-0.172	0.233	108.8	5.23
2½	-0.215	0.194	108.7	7.31
3	-0.258	0.155	108.5	9.61
3½	-0.300	0.116	108.3	12.1
4	-0.343	0.077	108.2	14.8
4½	-0.386	0.038	108.0	17.7
5	-0.429	-0.002	107.8	20.7
5½	-0.472	-0.041	107.7	23.9
6	-0.515	-0.080	107.5	27.2
6½	-0.558	-0.119	107.3	30.7
7	-0.601	-0.158	107.2	34.3
7½	-0.644	-0.198	107.0	38.0
8	-0.687	-0.237	106.8	41.9
8½	-0.730	-0.276	106.7	45.8
9	-0.773	-0.315	106.5	50.0
9½	-0.815	-0.354	106.3	54.2
10	-0.858	-0.393	106.2	58.5

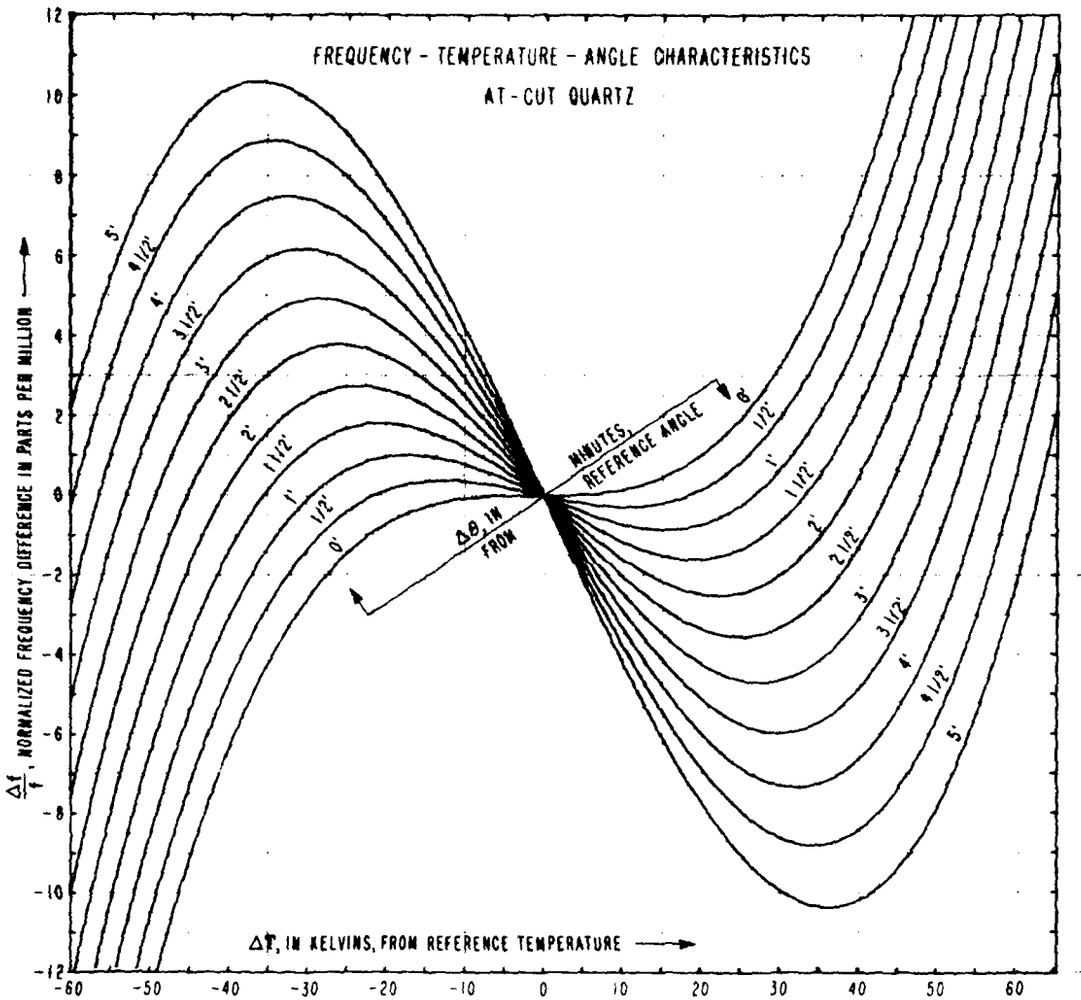

FIGURE 8. FREQUENCY-TEMPERATURE-ANGLE CHARACTERISTICS OF AT-CUT QUARTZ

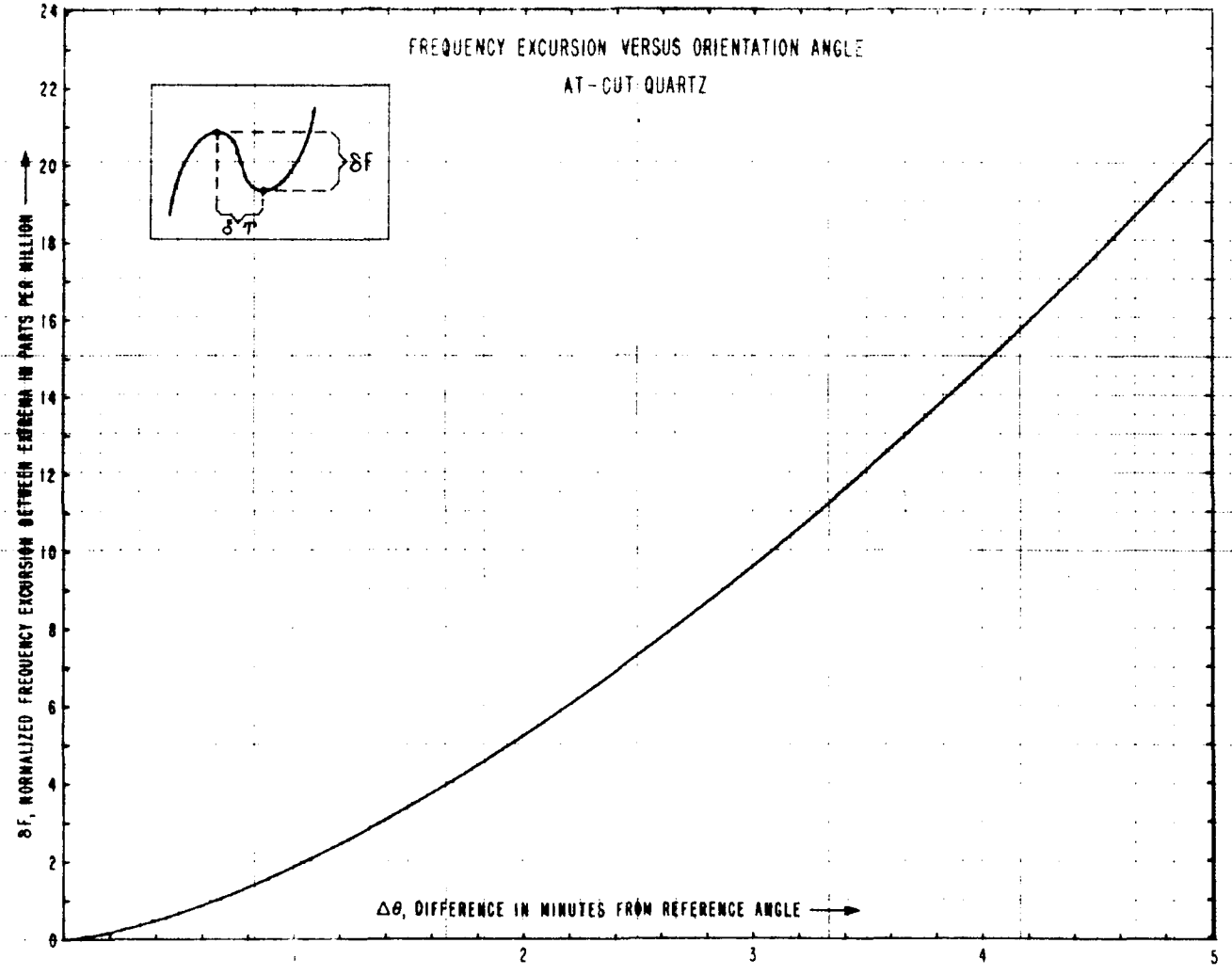

FIGURE 9. FREQUENCY EXCURSION VERSUS ORIENTATION ANGLE FOR AT-CUT QUARTZ RESONATORS.

The slight differences in the second- and third-order coefficients, at the reference angle, between Table 2 and Table 3 are indicative of the changes encountered due to electrical operating conditions.

From the data in Table 3, obtained from the relation

$$\delta f = 4(b^2 - 3ac)^{3/2}/27c^2, \tag{35}$$

the curve of Figure 9 may be obtained. If δT is defined as the temperature interval corresponding to δf, then δT and δf are found to be related by the simple relation

$$\delta f = (c/2) \cdot (\delta T)^3, \tag{36}$$

where c is a function of orientation. In Figure 10, (36) has been plotted for the average value of (c/2) from Table 3.

The frequency-temperature-angle characteristics for ST-cut quartz are shown in Figure 11. The angle indicated is θ; since, from Table 2, the first-order temperature coefficient is less sensitive to changes in Φ than in θ by a factor of 21, the curves of Figure 11 also indicate approximately the behavior with respect to $\Delta\Phi$ changes of 21'. From the curves, one sees that the SC-cut is flatter than the corresponding AT-cut, and that an AT-cut operating about its upper turning point would be replaced by an SC-cut operating about its lower turning point. For TCXO operation, the SC-cut is more difficult to pull than the AT-cut because the SC-cut's capacitance ratio is about a factor of three higher than the AT-cut's, as may be seen from Table 1.

Harmonic Effect

Changing the harmonic of operation is similar, as far as the resonance frequency-temperature behavior is concerned, to a change in apparent orientation angle, [43-46] except that the harmonic effect is quantized. Figure 12 shows the behavior of the resonance frequency for an AT-cut resonator at M = 1, 3, and 5; the curve marked "∞" corresponds to the resonance frequency at an indefinitely high harmonic, or at any of the harmonics of the antiresonance frequency.

The relation for the difference between the first-order temperature coefficients of the resonance and antiresonances was derived by Onoe;[47] the equations for the higher-order differences were obtained recently.[43,44] For the first-order we have

$$T_X = T_{fRo}^{(M)} - T_{fAo}^{(1)} = -G_o \cdot T_k, \tag{37}$$

where

$$G_o = +2k^2/((X_{Ro}^{(M)})^2 + k^2(k^2 - 1)), \tag{38}$$

and where T_k is the first-order temperature coefficient of piezoelectric coupling. The harmonic effect arises from the root $X_{Ro}^{(M)}$ appearing in (38). Figure 13 presents G_o as function of k and M. It is seen, from (37) and (38), that for $M \gg 1$, $G_o \to 0$, and $T_{fRo} \to T_{fAo}$ as shown in Figure 12.

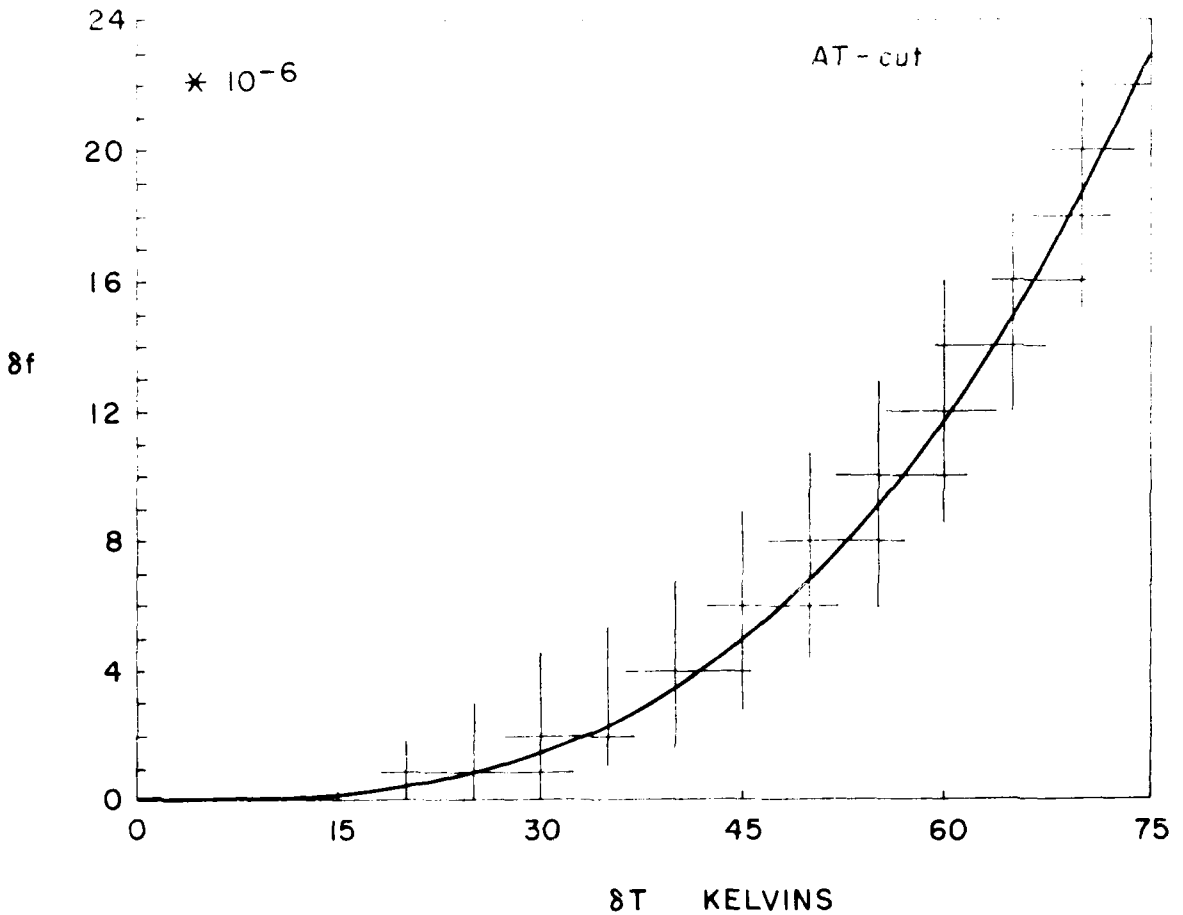

FIGURE 10. FREQUENCY EXCURSION VERSUS TEMPERATURE EXCURSION.

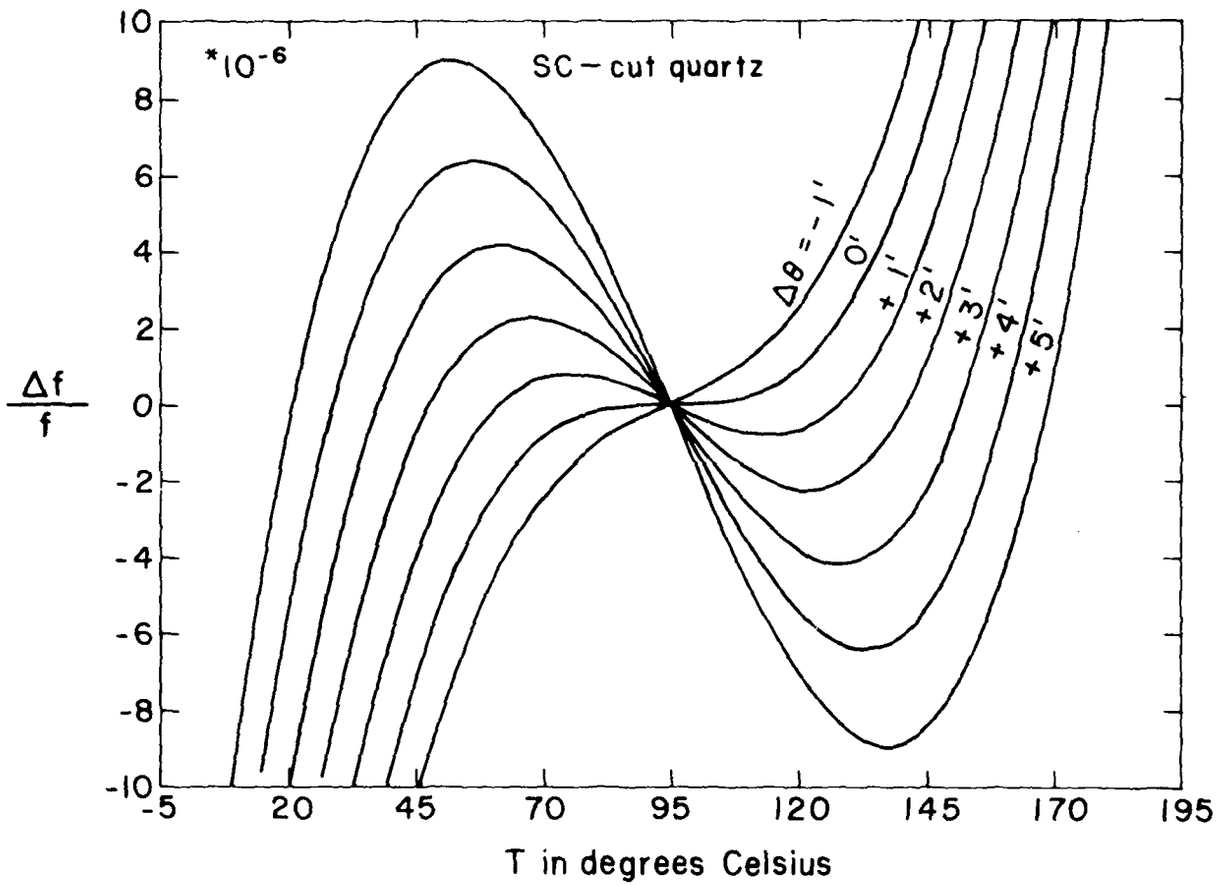

FIGURE 11. FREQUENCY-TEMPERATURE-ANGLE CHARACTERISTICS OF SC-CUT QUARTZ RESONATORS.

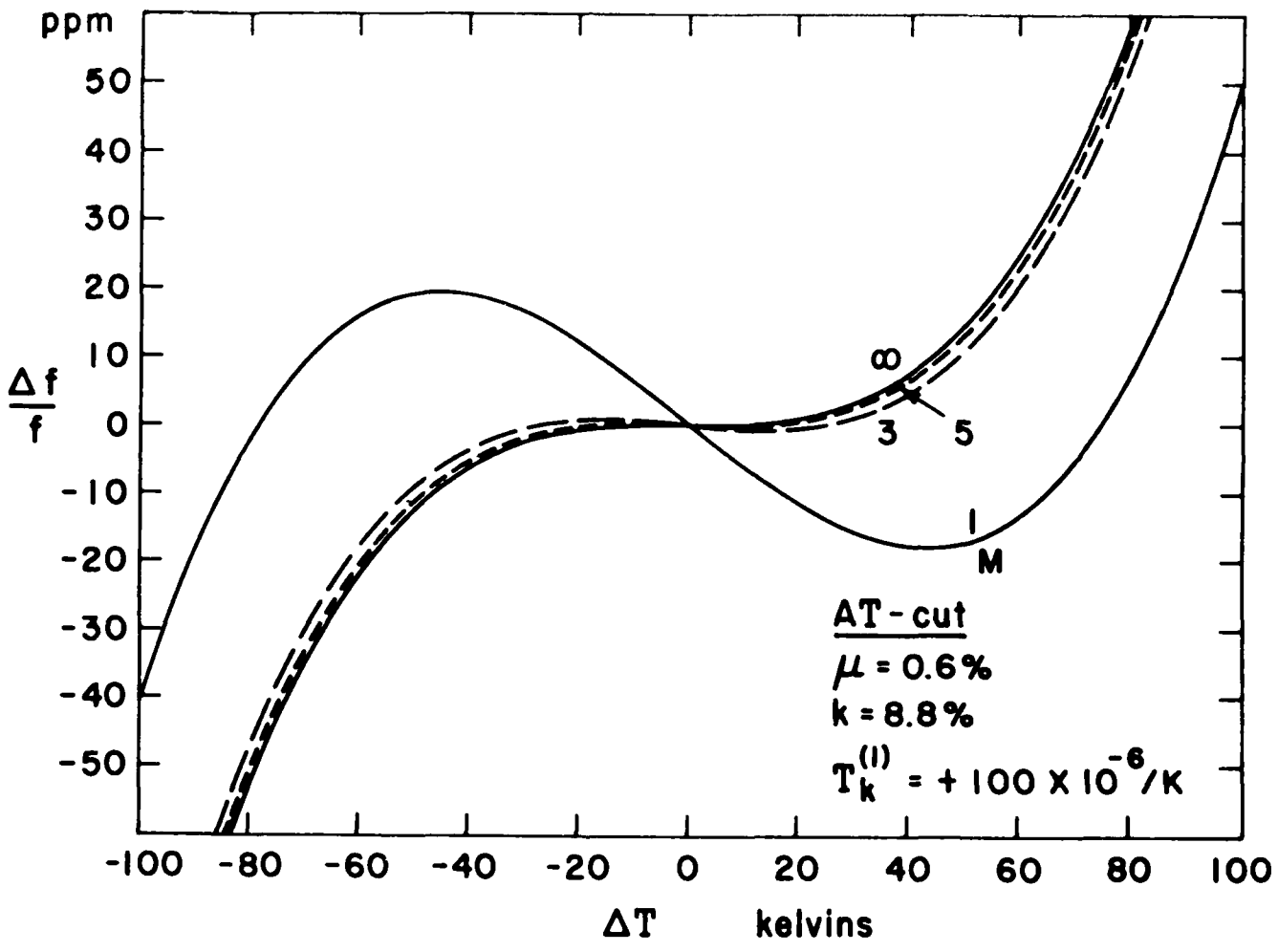

FIGURE 12. FREQUENCY-TEMPERATURE-HARMONIC CHARACTERISTICS OF AT-CUT QUARTZ RESONATORS.

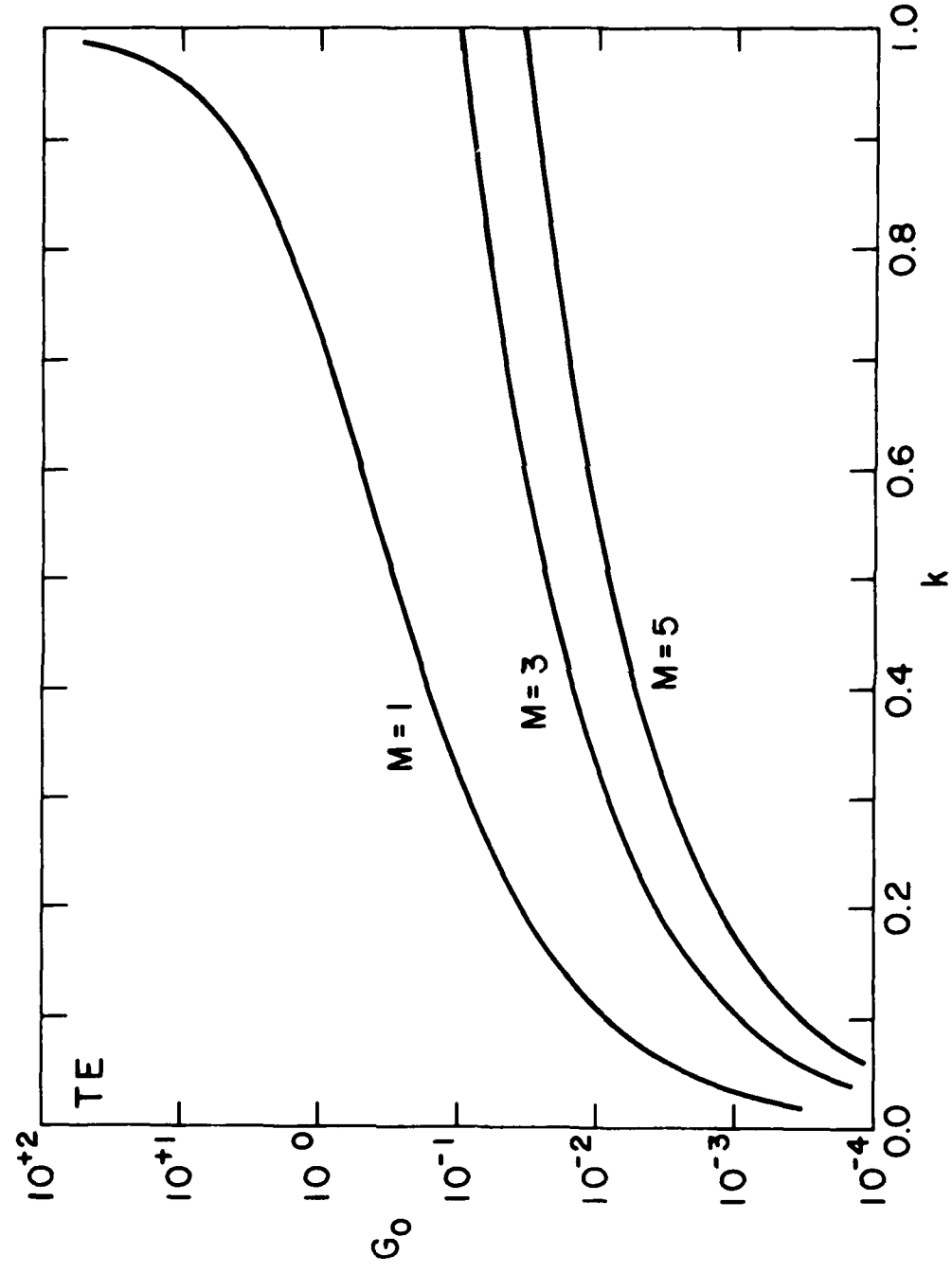

FIGURE 13. ONOE FUNCTION VERSUS COUPLING.

Load Capacitor Effect

Series load capacitor insertion is described in regard to its effect on k by (11); with respect to its influence on temperature behavior, (37) may be used with k_L^2 from (38), along with the relation between T_{kL} and T_k. This is found to be

$$2T_{kL} = 2T_k + \alpha(T_{CL} - T_{Co}), \tag{39}$$

meaning that the temperature behavior of C_L now comes into play, along with that of C_o. Values for T_{Co}, T_k, and T_X are given in Table 2 for the AT- and SC-cuts. With α and k^2 known, Figure 13 can be used to find $G_o(k_L)$.

The load capacitor effect on frequency-temperature behavior is given in Figure 14 for the SC-cut and a representative value of α; the curve for the AT-cut is shown in Figure 22, in connection with a numerical example.

Mass-Loading Effect[45,46]

Addition of mass-loading results in an expanded form of (37):

$$T_X = T_{fR\mu}^{(M)} - T_{fA\mu}^{(1)} = -(2k^2 \cdot T_k + \mu(X_{R\mu}^{(M)})^2 \cdot T_\mu)/D, \tag{40}$$

where

$$D = (X_{R\mu}^{(M)})^4\mu^2 + (X_{R\mu}^{(M)})^2(2\mu k^2 + \mu + 1) + k^2(k^2 - 1), \tag{41}$$

and T_μ is the temperature coefficient of the normalized mass-loading.

$$T_\mu = -T_\rho - T_h, \tag{42}$$

Where $T_\rho = -(\alpha(X_1'') + \alpha(X_2'') + \alpha(X_3''))$ is the temperature coefficient of density and $T_h = +\alpha(X_2'')$ is the temperature coefficient of expansion in the thickness (X_2'') direction. The thermoelastic constants $\alpha(X_i'')$ for quartz are given in Table 2.

The quantity multiplying T_k in (40) is called the Onoe function:[46]

$$G_\mu^{(M)} = +2k^2/D.$$

G_μ is plotted versus μ for various k values and for M = 1, 3, and 5 in Figures 15, 16, and 17, respectively. For AT-cut quartz, G_μ is plotted as function of μ for various harmonics in Figure 18.

By means of (40) and the numerical value for $\partial a/\partial\theta$ provided in Table 2, one may convert changes in "a" due to changes in μ and/or M into apparent angle changes. In Figure 19 the angle shift with mass-loading, from the $\mu = 0$ value, is plotted as function of μ with M the parameter. In Figure 20 the apparent angular shift for transitions between harmonics is shown as function of μ; both figures are for AT-cut quartz.

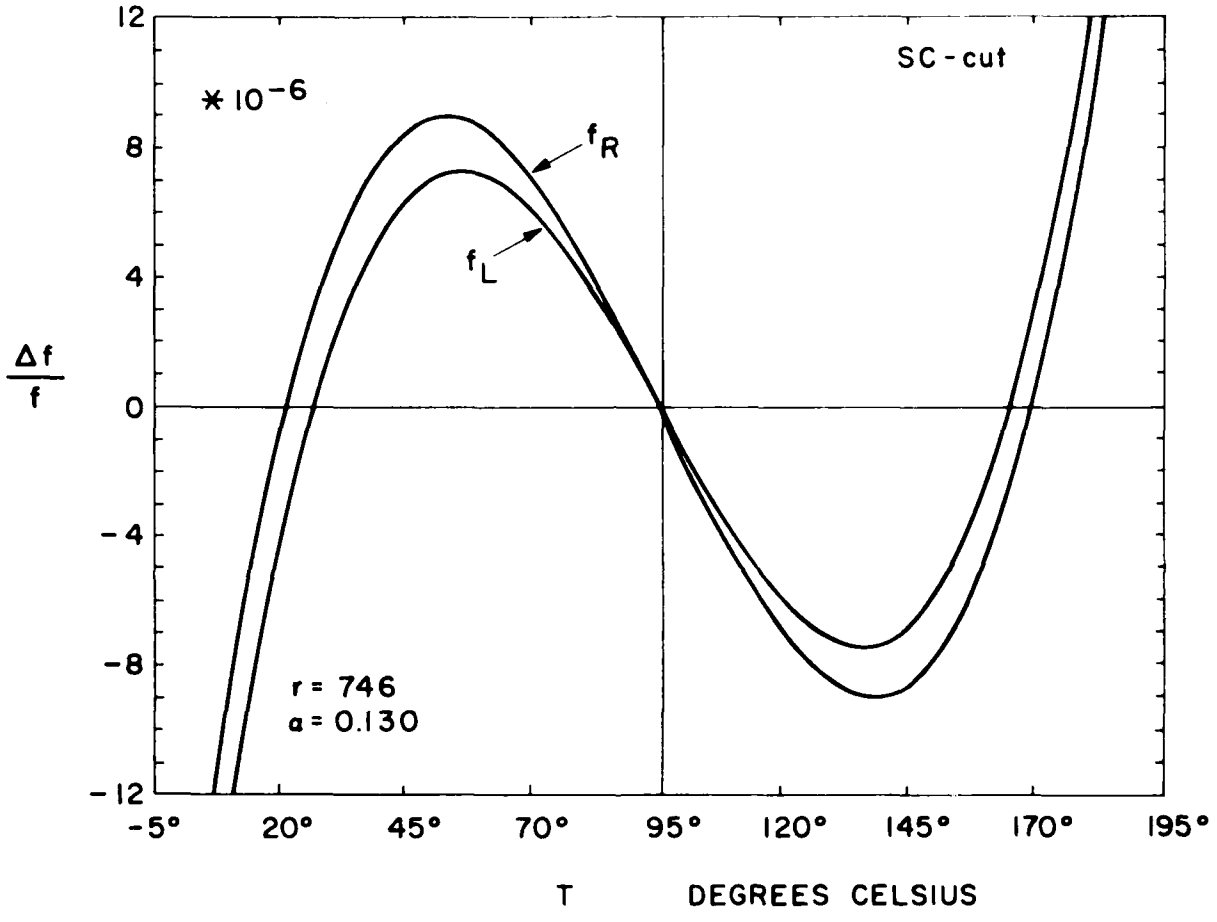

FIGURE 14. FREQUENCY-TEMPERATURE-LOAD CAPACITANCE CHARACTERISTIC FOR AN SC-CUT RESONATOR.

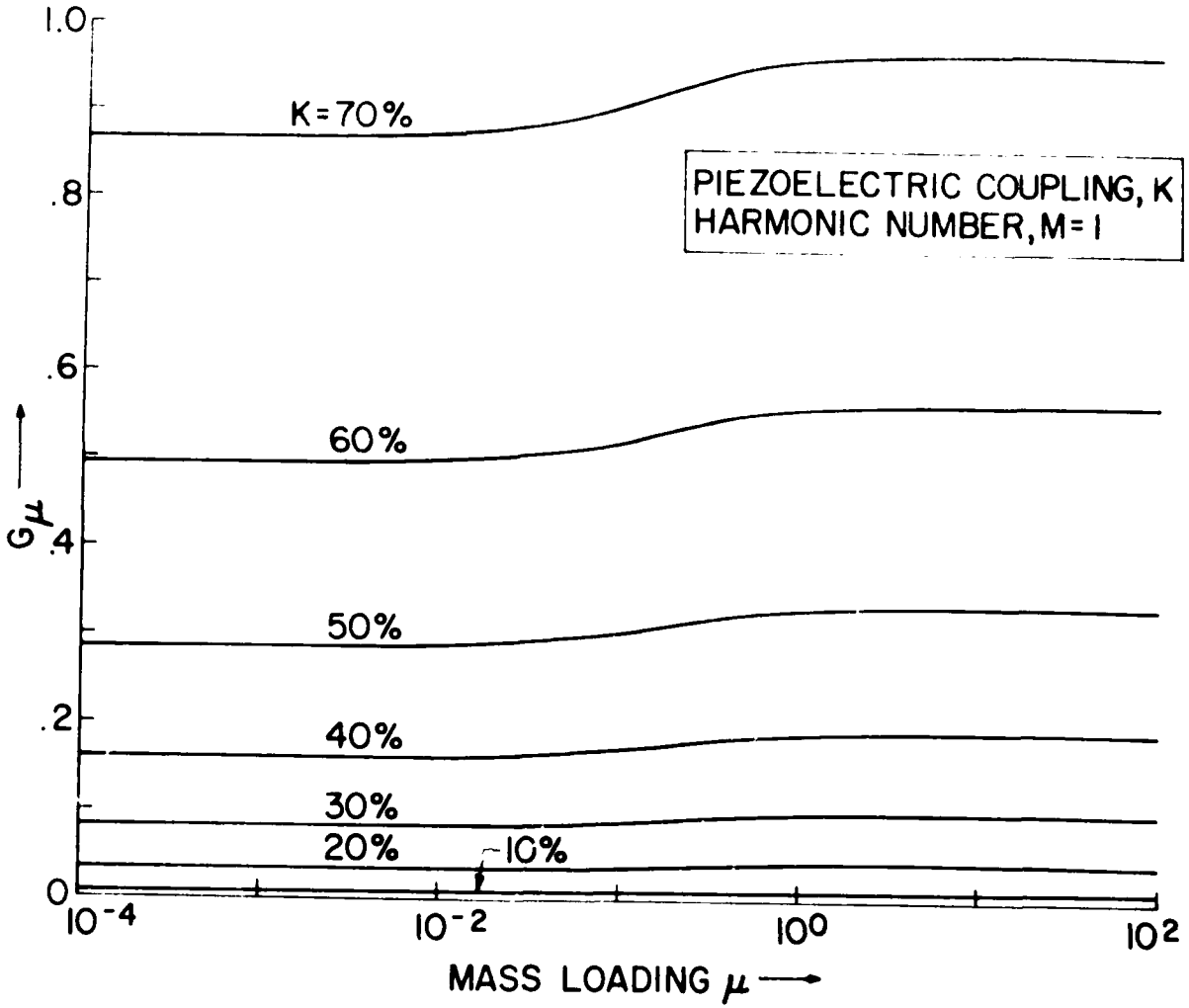

FIGURE 15. ONOE FUNCTION VERSUS MASS-LOADING FOR M = 1 .

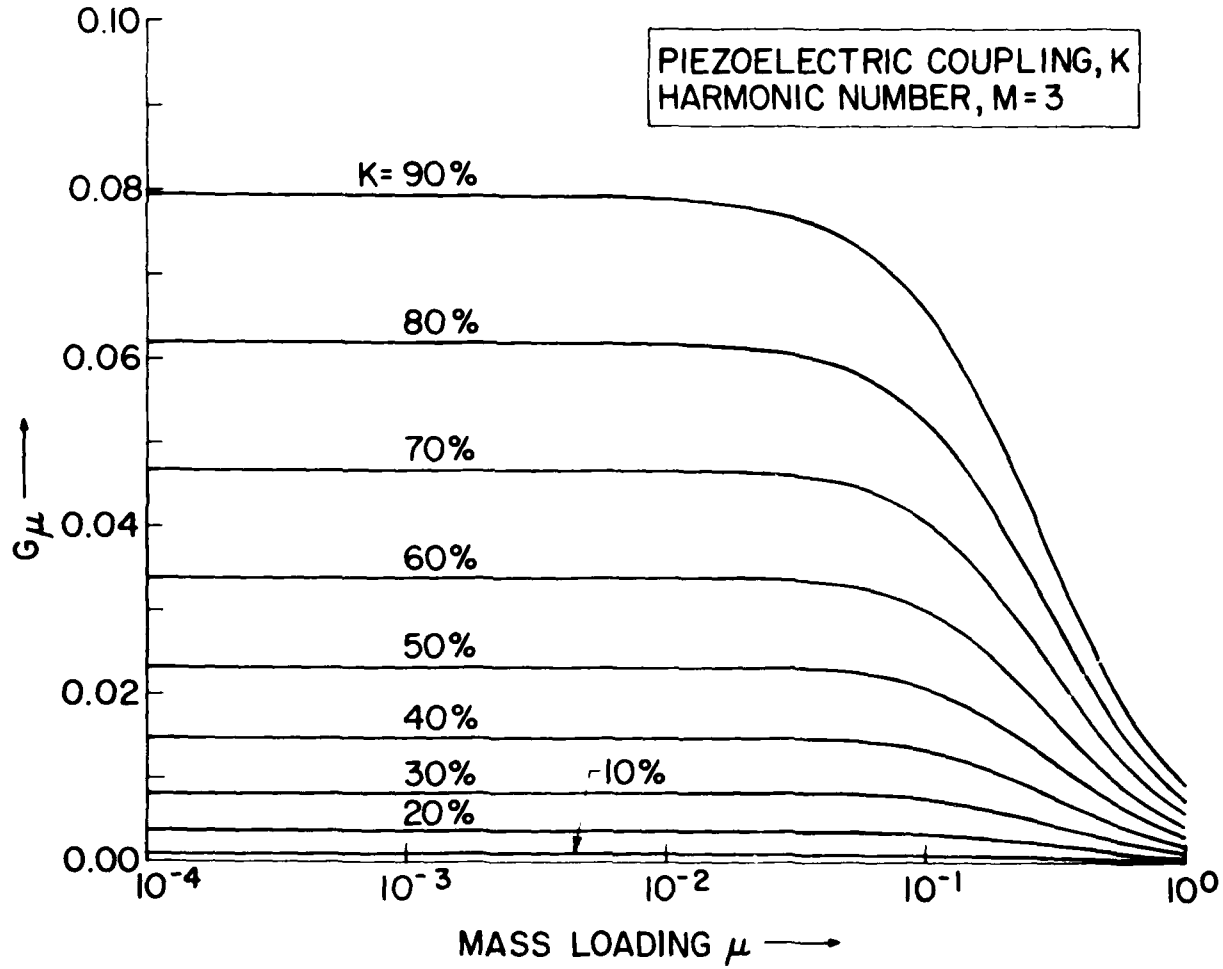

FIGURE 16. ONOE FUNCTION VERSUS MASS-LOADING FOR M = 3.

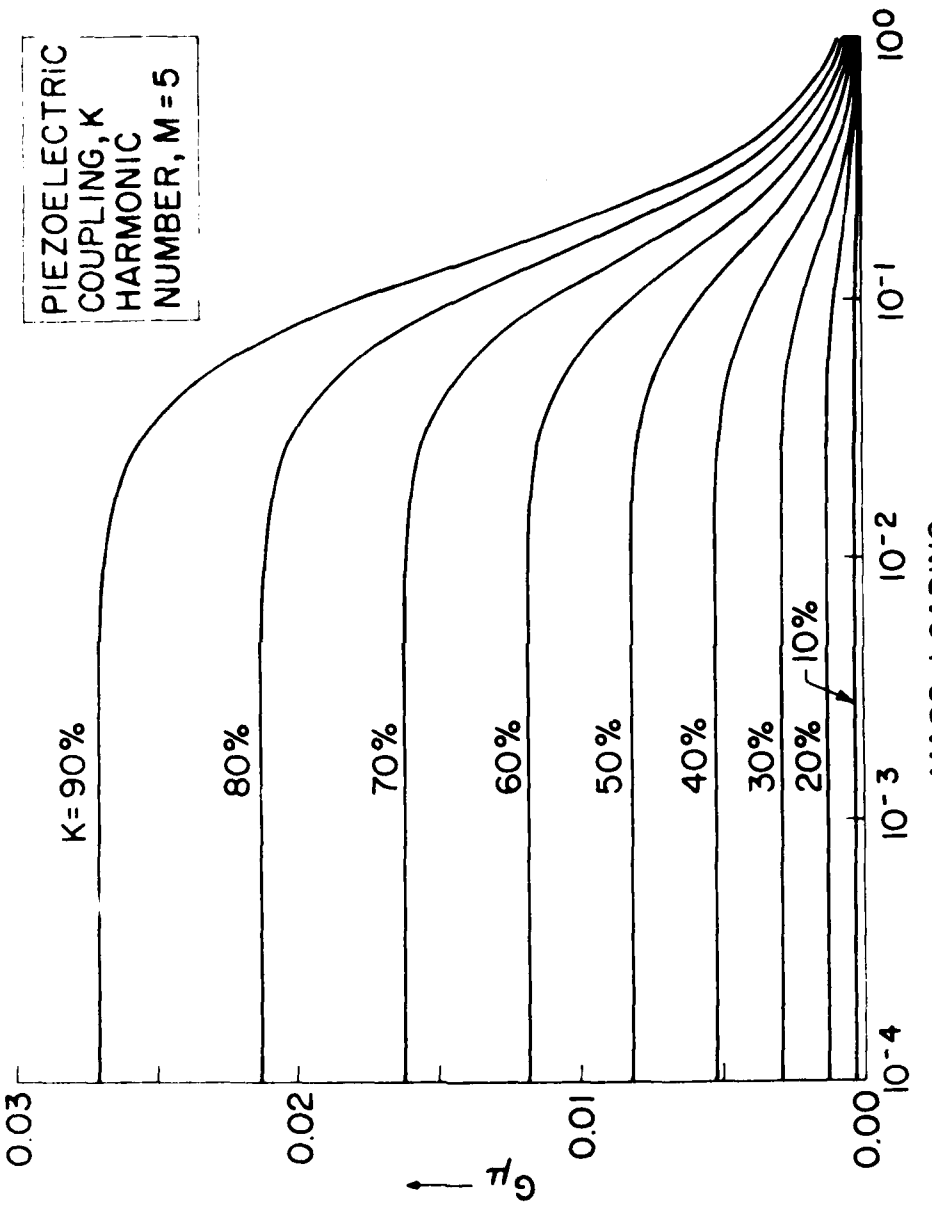

FIGURE 17. ONOE FUNCTION VERSUS MASS-LOADING FOR M = 5.

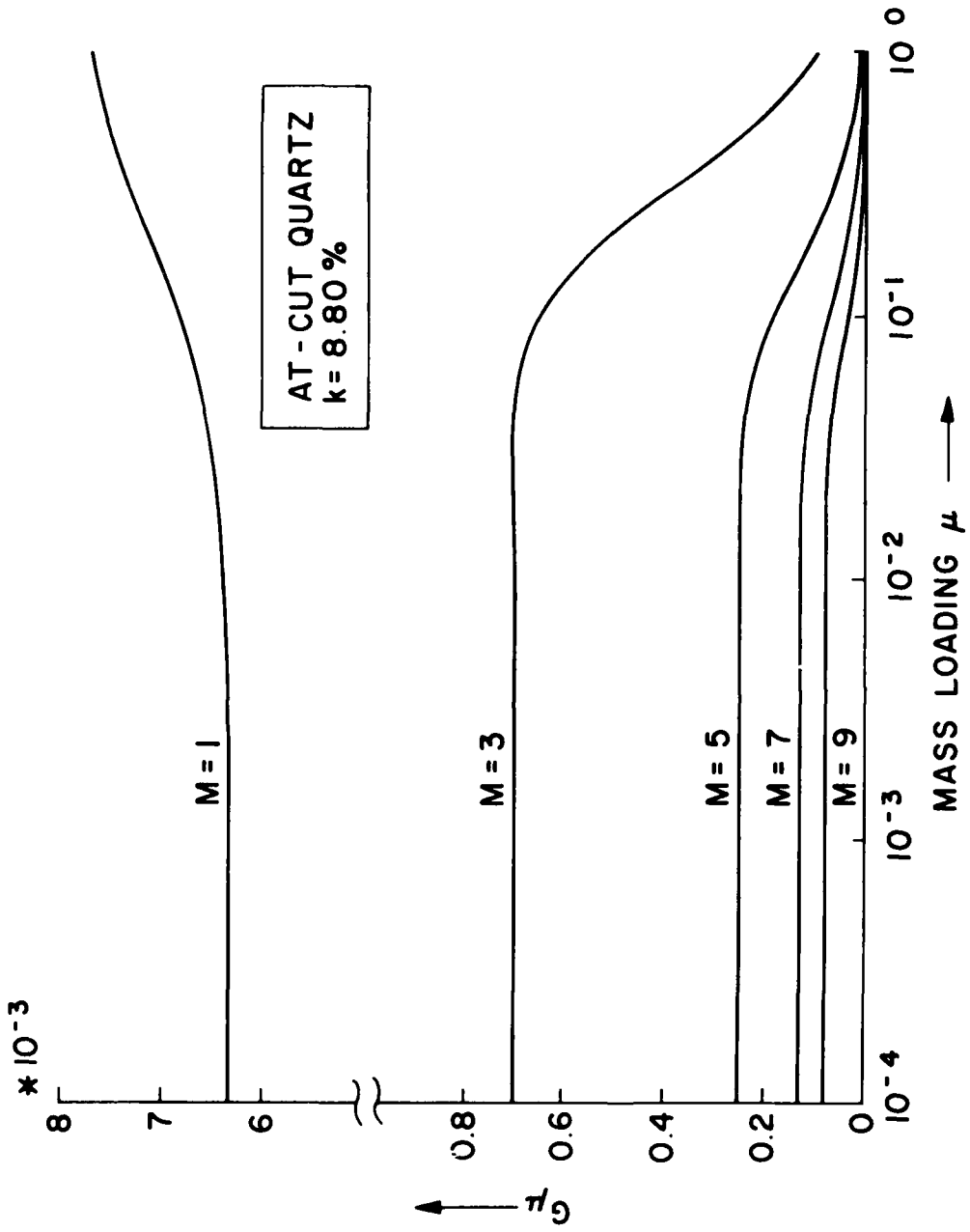

FIGURE 18. ONOE FUNCTION VERSUS MASS-LOADING FOR AT-CUT QUARTZ.

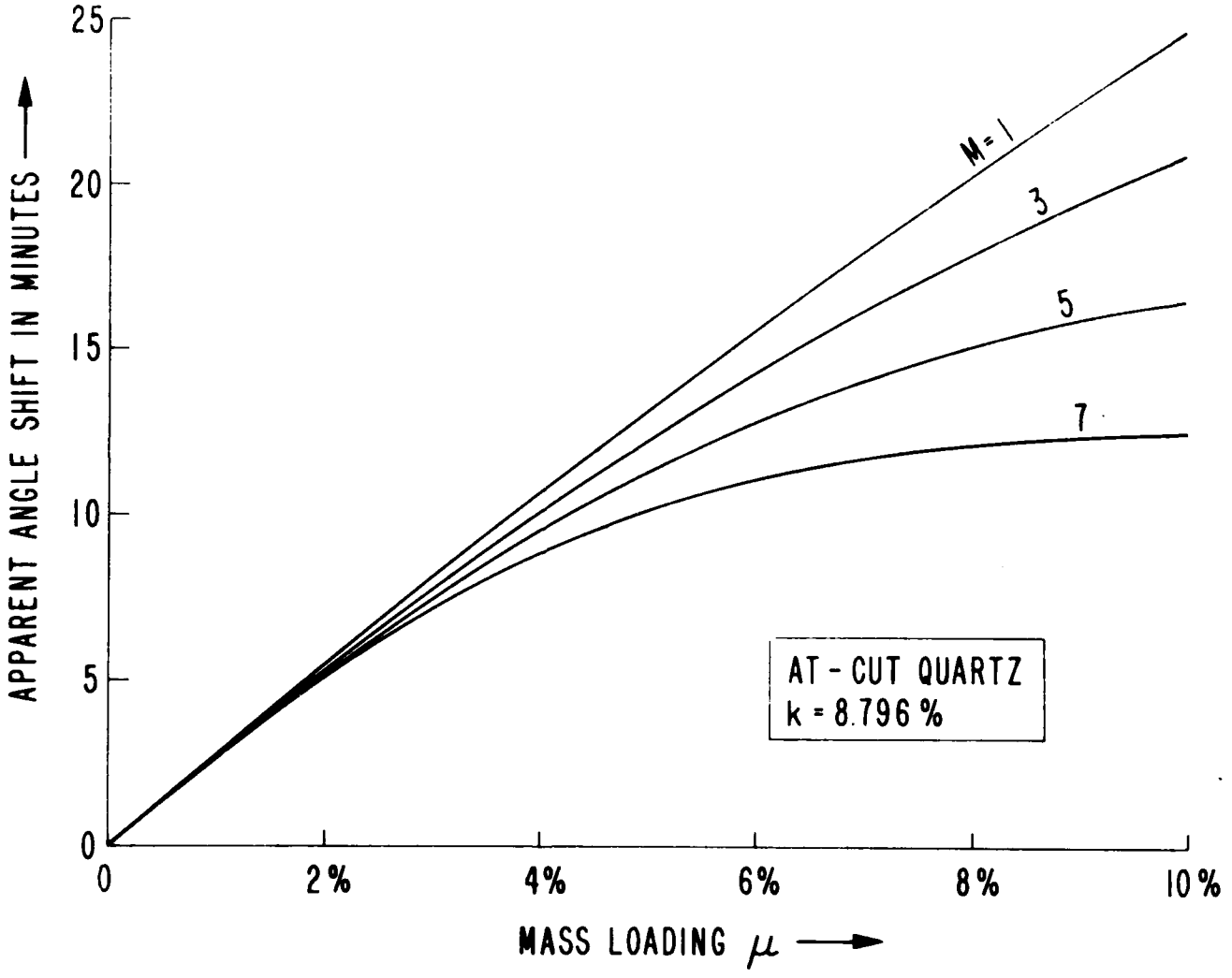

FIGURE 19. APPARENT ANGLE SHIFT VERSUS MASS-LOADING FOR VARIOUS HARMONICS.

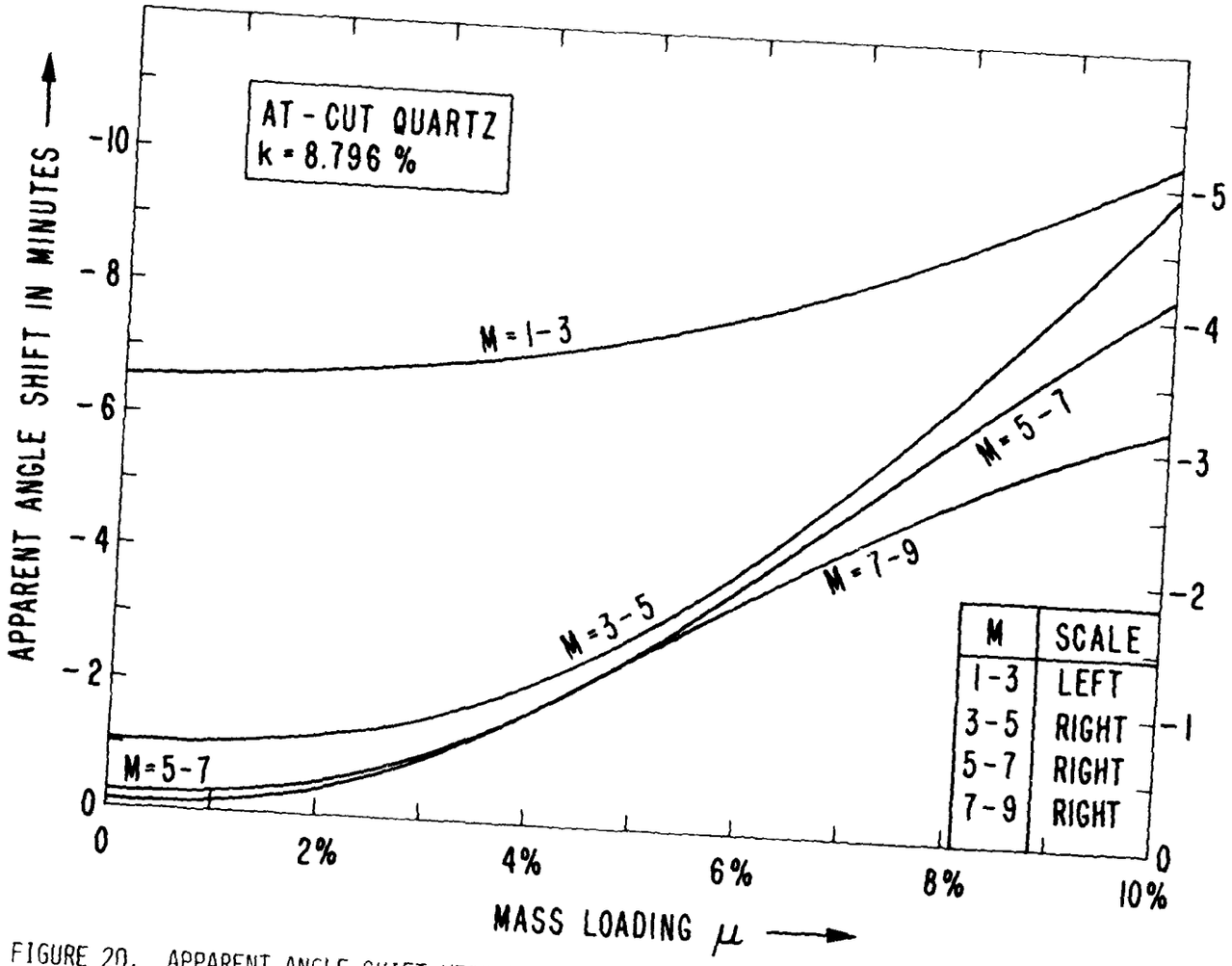

FIGURE 20. APPARENT ANGLE SHIFT VERSUS MASS-LOADING FOR TRANSITIONS BETWEEN HARMONICS.

Inclusion of the C_L effect for the mass-loading case is made by writing (40) twice--once for $k \triangleq k_1$, $\mu = \mu_1$, and harmonic = N, and then for k_2, μ_2, and M, and subtracting. The result is

$$T_{fR\mu 2}^{(M)} - T_{fR\mu 1}^{(N)} = [-2k_2^2 Tk_2/D_2^{(M)} + 2k_1^2 Tk_1/D_1^{(N)}] + [-(\mu_2 X_{R\mu 2}^2/D_2)^{(M)} + (\mu_1 X_{R\mu 1}^2/D_1)^{(N)}] \cdot T_\mu. \quad (44)$$

One now uses (11) and (39) to relate k_1 and k_2, Tk_1 and Tk_2. Equation (44) then incorporates the full effects of changes of α, μ, and harmonic on the first-order resonance-frequency/temperature coefficient.

EQUIVALENT CIRCUIT CONSIDERATIONS

The equivalent circuit of Figure 21 is usually used to represent a crystal resonator in the vicinity of a harmonic.[48] C_o is given by (2), while

$$C_1^{(M)} = 8\, C_o k^2/\pi^2 M^2, \quad (45)$$

$$R_1^{(M)} = \tau_1/C_1^{(M)} = \pi^2 M^2 \eta/8\, C_o k^2 \bar{c}, \quad (46)$$

and

$$L_1 = \pi M^2/32\, C_o k^2 (f_{Ro}^{(M)})^2. \quad (47)$$

The quantity τ_1 is the motional time constant,[49]

$$\tau_1 = \eta/\bar{c} \quad (48)$$

η is the acoustic viscosity, and $\bar{c}$ is the piezoelectrically-stiffened elastic constant. It is convenient to define two quantities that contain no geometrical factors, but which are functions of material only. These are the motional capacitance and motional resistance constants:

$$\Gamma_1^{(M)} = C_1^{(M)} \cdot 2h/A = \varepsilon/rM^2, \quad (49)$$

$$P_1^{(M)} = R_1^{(M)} \cdot A/2h = \tau_1/\Gamma_1^{(M)}. \quad (50)$$

In (49), r is the capacitance ratio

$$r^{(M)} = C_o/C_1^{(M)} = \tfrac{1}{2} \cdot (\pi M/2k)^2. \quad (51)$$

Table 1 lists values for ε, $\bar{c}$, η, τ_1, r, Γ_1, P_1, and $N = v/2 = (\bar{c}/\rho)^{1/2}/2$; quantities appearing without a superscript (M) are for M = 1. The dimensionless number Ψ appearing in Table 1 is a form factor that takes into account the nonuniform distribution of motion with lateral distance along the plate.[30,32] The effective value of $C_1^{(M)}$ is just Ψ times the value obtained from (45); whereas $R_1^{(M)}$ is divided by Ψ to get the effective motional resistance. The static capacitance, C_o, is not affected by the motional distribution.

Introduction of a series load capacitor alters C_o according to (10); it also changes the other circuit parameters:[31]

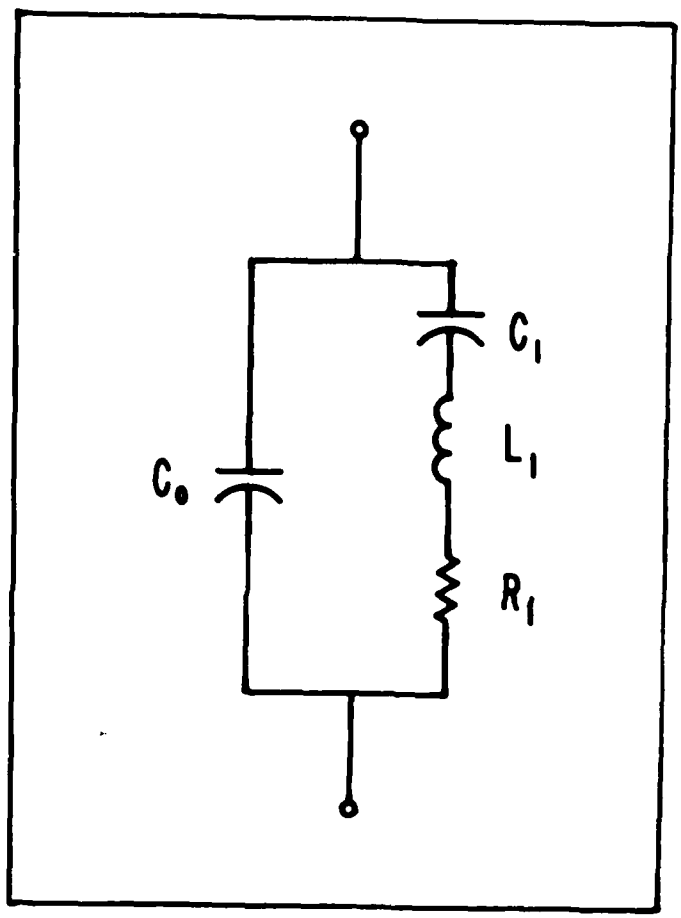

FIGURE 21. BUTTERWORTH-VAN DYKE EQUIVALENT CIRCUIT.

$$C_{1L} = C_1(1 - \alpha)^2, \tag{52}$$

$$R_{1L} = R_1/(1 - \alpha)^2, \tag{53}$$

$$L_{1L} = L_1/(1 - \alpha)^2, \tag{54}$$

$$r_L = r/(1 - \alpha). \tag{55}$$

From the definitions (45) - (51), the temperature coefficients of the circuit parameters may be obtained in terms of those of the material coefficients. At present the quantity Tη is very imperfectly known.

FREQUENCY-TEMPERATURE-LOAD CAPACITANCE APPROXIMATIONS

To supplement the frequency approximations given in an earlier section, we give here those appropriate to the description of temperature behavior.

From Figures 15, 16, and 17, it is seen that the dependence of G_μ on μ is very weak until μ exceeds several percent; accordingly, it is usually acceptable to let $G_\mu = G_o$. The zeroth approximation to G_o is

$$G_o \simeq + 2k^2/(\pi M/2)^2 - 1/r; \tag{56}$$

the first approximation is

$$G_o \simeq + 2k^2/[(\pi M/2)^2 - k^2]. \tag{57}$$

The presence of μ only enters the second approximation:

$$G_\mu \simeq + 2k^2/\{(\pi M/2)^2[1 - \mu - (\frac{2k}{\pi M})^2]^2 + k^2(k^2 - 1)\}. \tag{58}$$

By making approximations of the sort found in (56) - (58), equation (44) may be reduced to various simpler forms. When $\alpha = 0$ and $\mu = 0$, one has

$$T_{fRo}^{(M)} - T_{fRo}^{(N)} = (Tr/2r) \cdot (1/M^2 - 1/N^2), \tag{59}$$

where

$$T_r = -2T_k. \tag{60}$$

If $\mu_1 \neq \mu_2$, $M \neq N$, then with the addition of C_L the exact result is

$$\begin{aligned} T_{fR\mu 2}^{(M)} - T_{fR\mu 1}^{(N)} = {} & -2k^2 T_k \cdot [(1 - \alpha)/D_2^{(M)} - 1/D_1^{(N)}] \\ & -k^2\alpha(1 - \alpha)(T_{CL} - T_{Co})/D_2^{(M)} \\ & -[(\mu X_R^2/D)_2^{(M)} - (\mu X_R^2/D)_1^{(N)}] \cdot T_\mu. \end{aligned} \tag{61}$$

The most important practical case is that where $\mu_2 = \mu_1 = \mu$, N = M. Then, for the shift in first-order temperature coefficient between resonance and load frequencies we have, approximately,

$$\begin{aligned} (T_{fR\mu} - T_{fL\mu}) \simeq {} & + \frac{\alpha}{2rM^2}\{(1 + 2\mu)[T_r + (1 - \alpha) \cdot (T_{CL} - T_{Co})] \\ & + 2\mu \cdot T\mu\}. \end{aligned} \tag{62}$$

For small μ this further reduces to

$$(T_{fRo} - T_{fLo}) \simeq \frac{+\alpha}{2rM^2} \cdot [Tr + (1 - \alpha) \cdot (T_{CL} - T_{Co})]. \tag{63}$$

From (27) and (11) the corresponding frequency shift is

$$\frac{(\Omega_{Lo}^{(M)} - \Omega_{Ro}^{(M)})}{M} \simeq \frac{4k^2 \cdot \alpha}{\pi^2 M^2} = \frac{\alpha}{2rM^2} . \tag{64}$$

USE OF AT- AND SC-CUT QUARTZ RESONATORS FOR TCXO APPLICATIONS

For the fundamental harmonic, M equals 1, and (64) becomes

$$(f_L - f_R)/f_R = \Delta f/f \simeq \alpha/2r. \tag{65}$$

This quantity is to be compared with δf from (35), which is shown in Figure 9 versus Δθ. Equation (35) may be approximated, in its explicit dependence upon Δθ, for the AT-cut, by

$$\delta f(\Delta\theta) \simeq 1.85 \times 10^{-6} \cdot (\Delta\theta)^{3/2}, \tag{66}$$

where Δθ is in minutes of arc; for the SC-cut the multiplier is 1.60×10^{-6}. Since ~~½r~~ greatly exceeds δf, it is apparent that only a small variation in C_L about its operating point is sufficient to bring about the necessary frequency compensation.

Two further questions arise, however: one concerns the shift in frequency-temperature behavior of the resonator in going from the condition of f_R to f_L; the other concerns the smaller shifts in the frequency-temperature characteristic attendant on the variations of C_L about its initial setting point. Lesser considerations, e.g., the further effects of μ, also arise. These points will now be taken up and considered from the standpoint of a practical example.

Consider a crystal resonator with the following characteristics:

f_R = 20 MHz, M = 1, AT-cut

C_o = 3.0 pF

C_1 = 12.5 fF

R_1 = 4Ω

μ = 2%

Δθ ≃ 4½ minutes of arc.

Table 3 and Figure 10 show that this Δθ value corresponds approximately to

$$\delta fR \simeq 18 \times 10^{-6}, \quad \delta T \simeq 69.4^{o}C,$$

stemming from the temperature coefficients

$$a = -0.386 \times 10^{-6}/K,$$

$$b = +0.038 \times 10^{-9}/K^2$$

$$c = +108.0 \times 10^{-12}/K^3.$$

Figure 22 presents the behavior of the resonance frequency f_R with temperature. Operation with series load capacitor

$$C_L = 20 \text{ pF}$$

at the frequency at which the combination exhibits zero reactance produces, as function of temperature, the curve marked f_L in Figure 22, assuming $(TC_L - TC_o)$ vanishes. The f_L curve is characterized as follows:

$$\alpha = C_o/(C_o + C_L) = 0.130;$$

the capacitance ratio is

$$r = C_o/C_1 = 240,$$

corresponding to an effective coupling factor

$$k_{eff} = \pi/(8r)^{\frac{1}{2}} \approx 7.2\%,$$

and a load coupling factor

$$k_L = k(1 - \alpha)^{\frac{1}{2}} \approx 6.7\%.$$

The ratios α and r are inserted into (63) to yield the new first-order coefficient

$$a = -0.332 \times 10^{-6}/K.$$

Coefficients b and c remain unchanged to good approximation, but with the "a" coefficient change the curve is made to appear with shifted angle difference

$$\Delta\theta \approx 4 \text{ minutes of arc},$$

and now

$$\delta f_L \approx 15 \times 10^{-6}, \quad \delta T \approx 65.4^{\circ}C.$$

According to (53) the resistance of the combination is

$$R_{1L} = R_1/(1 - \alpha)^2 \approx 5.3\ \Omega.$$

If (35) is used, with "a" taken to depend upon α according to (62), then δf_L may be plotted against α for assumed values of $(TC_L - TC_o)$ and μ. Starting values of "a," with corresponding b and c values, may be taken from Table 3 for any choice of $\Delta\theta$. The resulting graphs are shown in Figure 23 for values pertinent to the example described above. In addition to the C_L value quoted (20 pF), two further values are indicated on the figure:

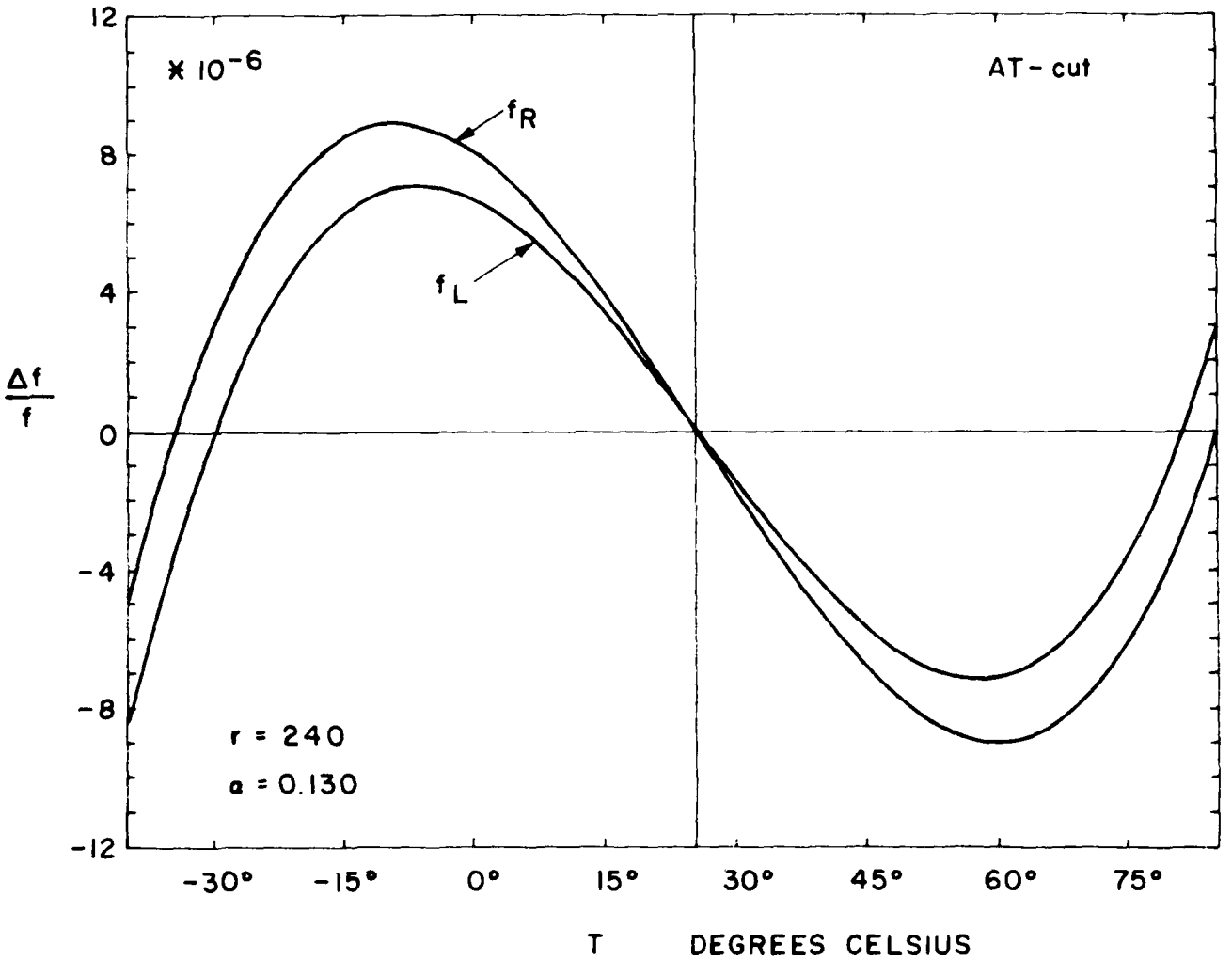

FIGURE 22. FREQUENCY-TEMPERATURE-LOAD CAPACITANCE CHARACTERISTIC FOR AN AT-CUT RESONATOR.

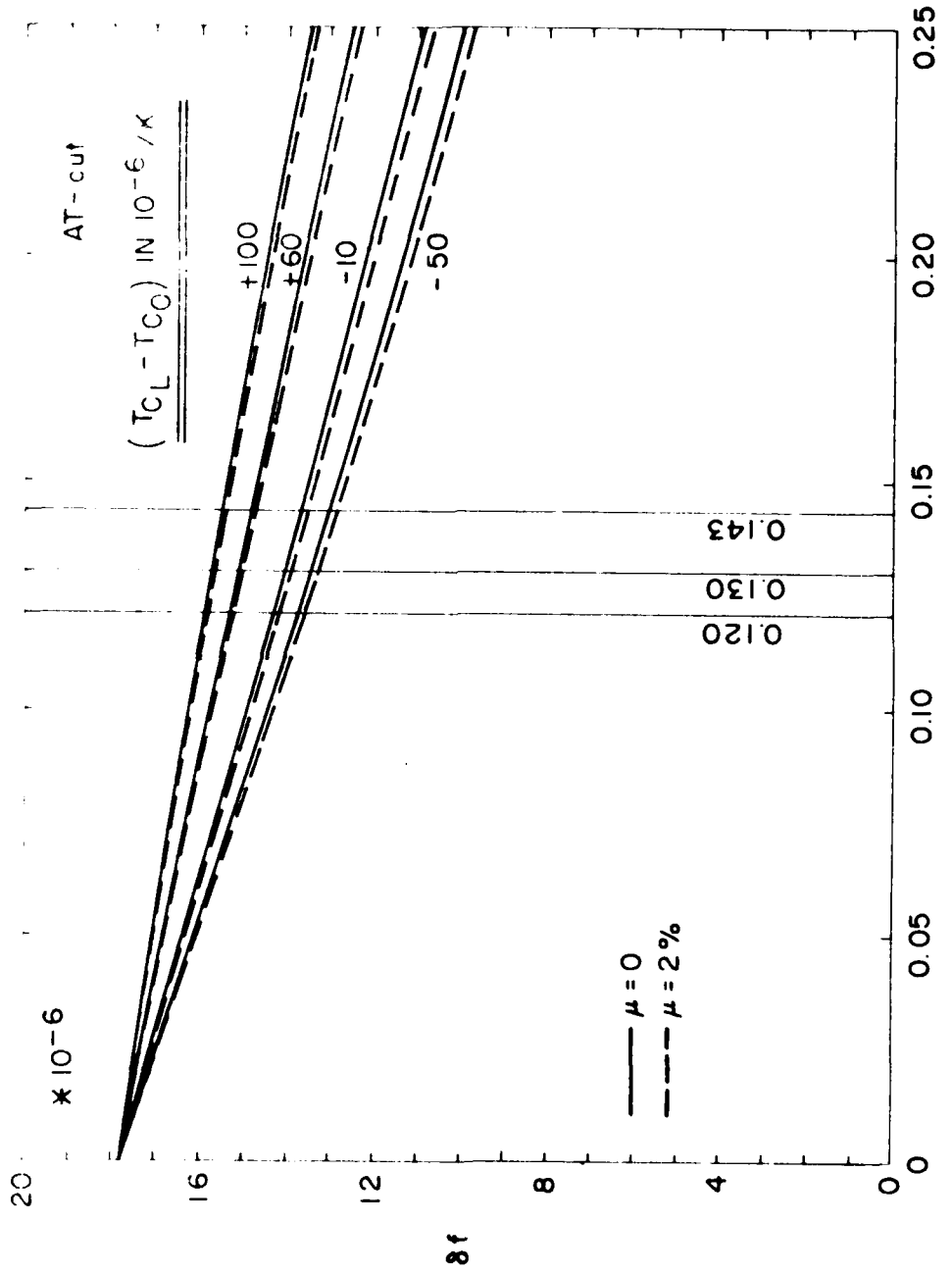

FIGURE 23. PORTION OF PETAL PLOT FOR AN AT-CUT RESONATOR.

$$C_L = 22 \text{ pF}, \quad \alpha = 0.120$$

and

$$C_L = 18 \text{ pF}, \quad \alpha + 0.143.$$

Graphs are plotted for the following values of $(TC_L - TC_o)$: -50, -10, +60, and +100, (all x $10^{-6}/K$), with and without the presence of 2% mass-loading. Inasmuch as the nominal value of TC_o for AT-cut quartz is

$$TC_o \approx +30 \times 10^{-6}/K,$$

(see Table 2), the assumed values of TC_L are:

$$\pm 20, +90, \text{ and } +130 \text{ (all x } 10^{-6}/K).$$

These figures correspond, respectively, to the nominal temperature coefficient values for ceramic capacitors, for porcelain micro-circuit capacitors, and for certain oscillator-varactor composites. TC_L is a function of reverse bias applied to a varactor;[20] one method for compensating this effect is to place a series diode in the bias circuit. Table 4 provides the δf_L values for the intersections of the three α values with the four $(TC_L - TC_o)$ graphs, with and without the presence of μ. From Figure 23 and Table 4, the relative sizes of the influences on δf_L may be discerned, and accommodated in the TCXO design.

Extensions of these plots to encompass the full range of α are given in Figures 24 to 39, for AT-cut crystals operating on the fundamental harmonic with capacitance ratios

$$r = 160 \ (20) \ 300,$$

angle shifts

$$\Delta\theta = 1 \ (10) \ 10 \text{ minutes of arc},$$

and temperature coefficient of capacitance differences

$$(TC_L - TC_o) = -100 \ (50) + 100 \times 10^{-6}/K.$$

Because the graphs for each value of $\Delta\theta$ conflue at $\alpha = 0$ and $\alpha = 1$ irrespective of $(TC_L - TC_o)$ the resulting design charts may be referred to as "petal plots." By their use, the shift of δf with α may be taken into account in TCXO applications.

CONCLUSIONS

The effective frequency-temperature curve of a crystal resonator operated with series load capacitance differs from that of the crystal alone. Since the principal method of compensating for the crystal frequency-temperature behavior in a TCXO employs series varactors and a temperature-sensitive compensation network, it is of major importance to be able to understand and deal with this effect in the design of TCXO's. The necessary formulas and discussion are given in this report.

TABLE 4.

TABLE OF St_L in 10^{-6} FOR VARIOUS VALUES OF α, μ, AND $(TC_L - TC_o)$

$(TC_L - TC_o)$ in 10^{-6}/K	μ (0% / 2%)	$\alpha = C_o/(C_o + C_L)$ = 0.120	0.130	0.143
	-50	13.74 / 13.60	13.43 / 13.28	13.03 / 12.87
	-10	14.30 / 14.18	14.03 / 13.90	13.67 / 13.53
	+60	15.30 / 15.22	15.09 / 15.00	14.82 / 14.72
	+100	15.88 / 15.83	15.71 / 15.65	15.49 / 15.41

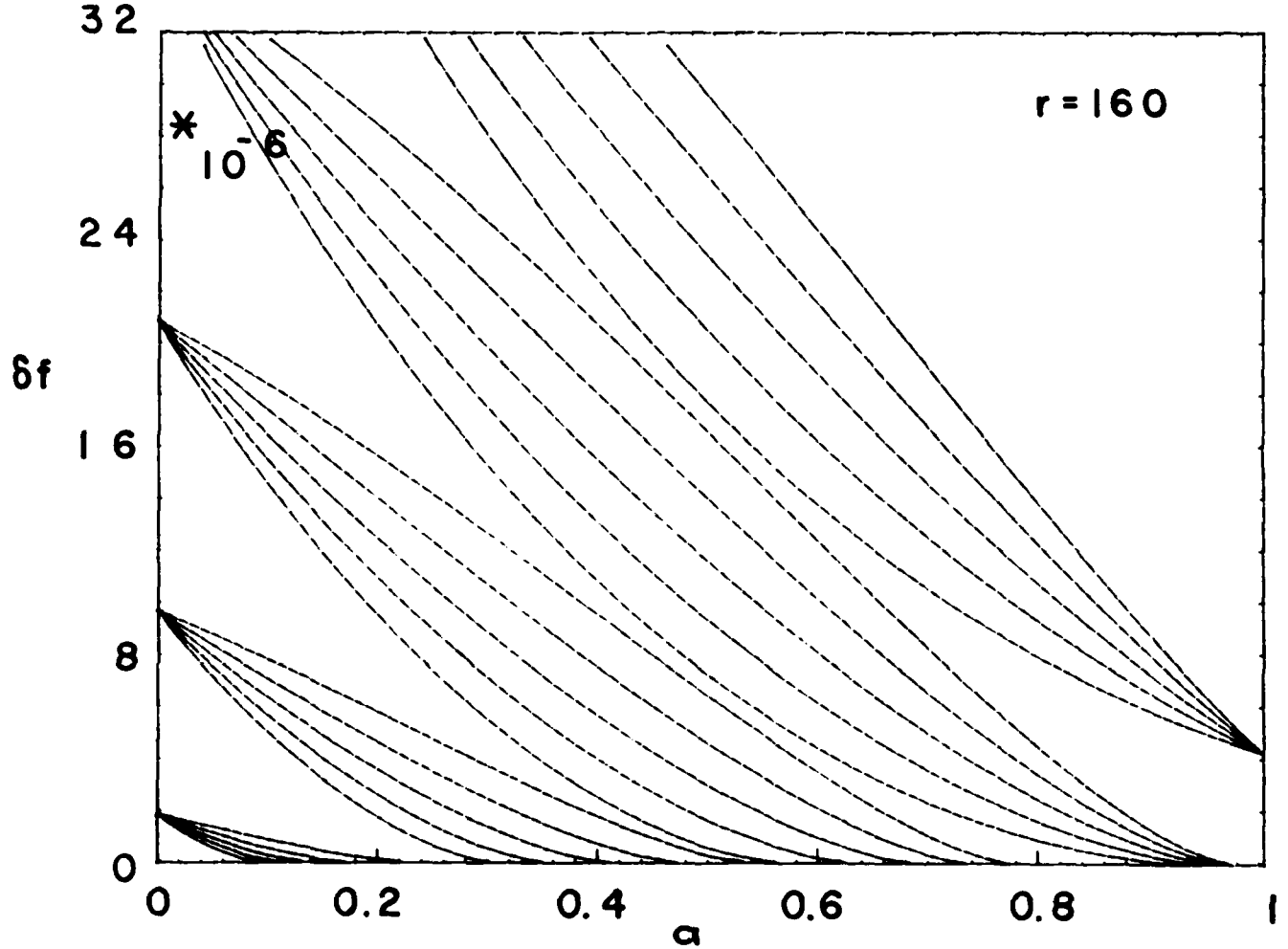

Figure 24. Petal plot of δf vs. α $\Delta\theta = 1'(2')\,9'$.

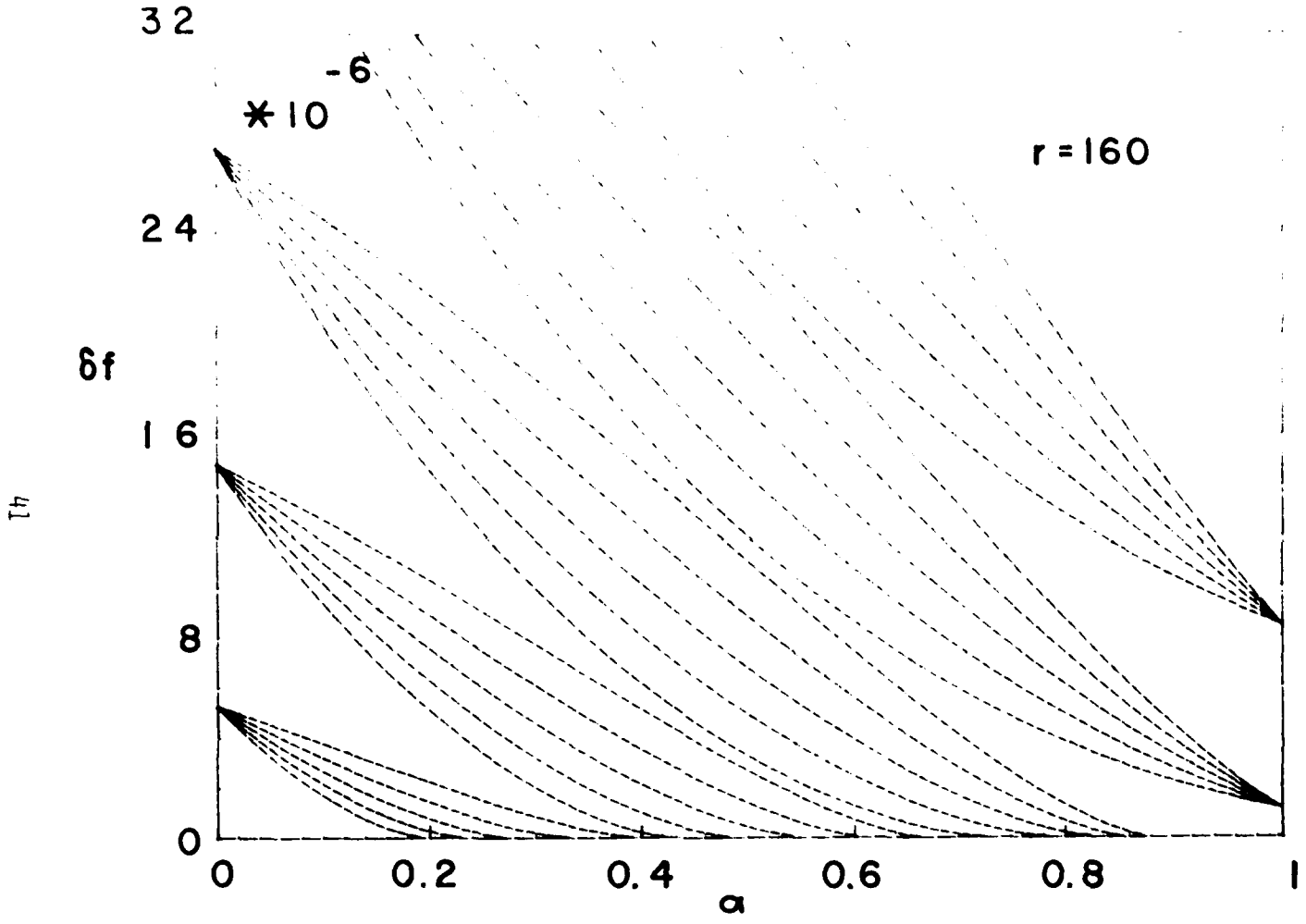

Figure 25. Petal plot of δf vs. α $\Delta\theta = 2'(2')10'$.

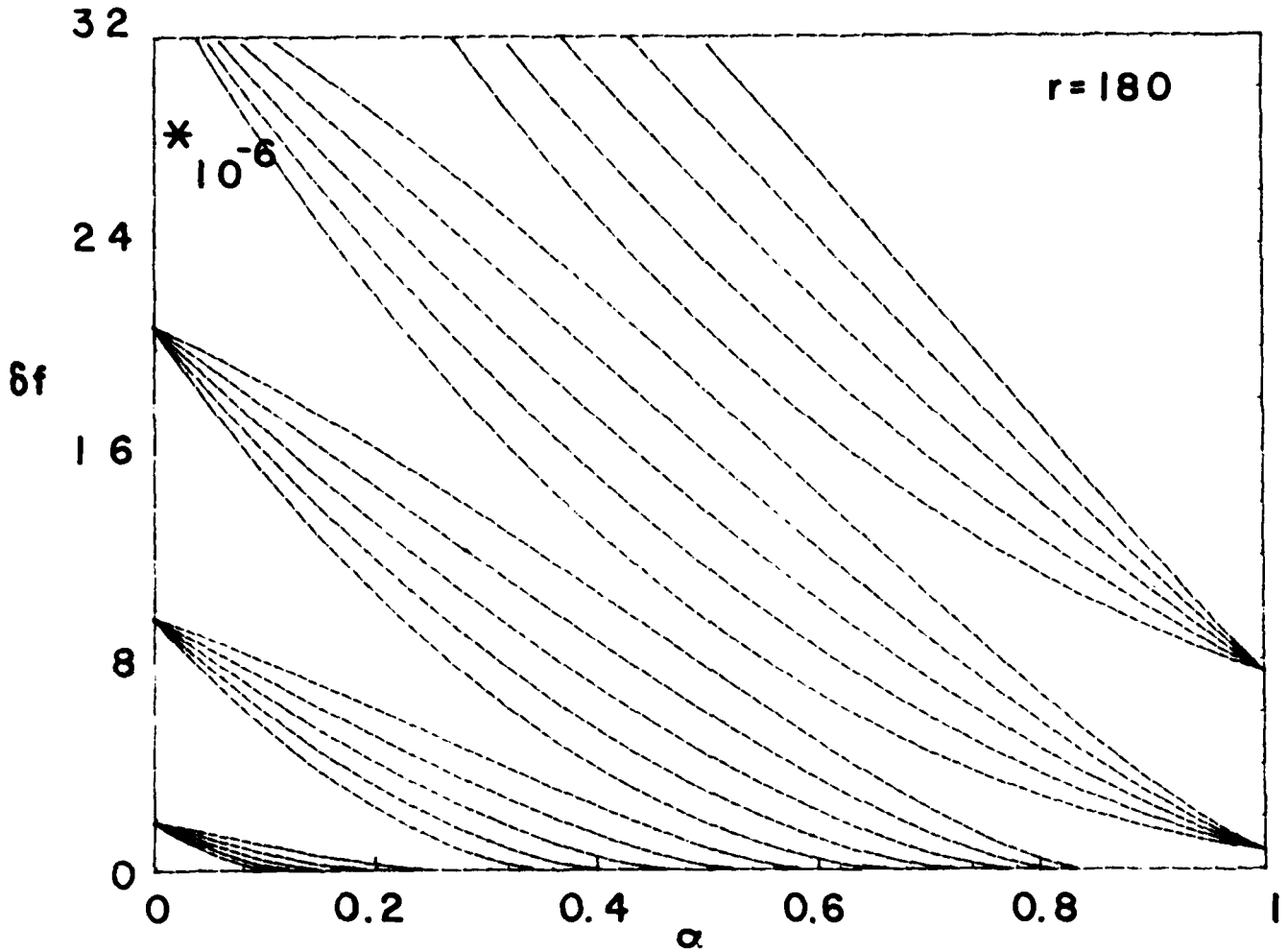

Figure 26. Petal plot of δf vs. α $\Delta\theta = 1'(2')\,9'$.

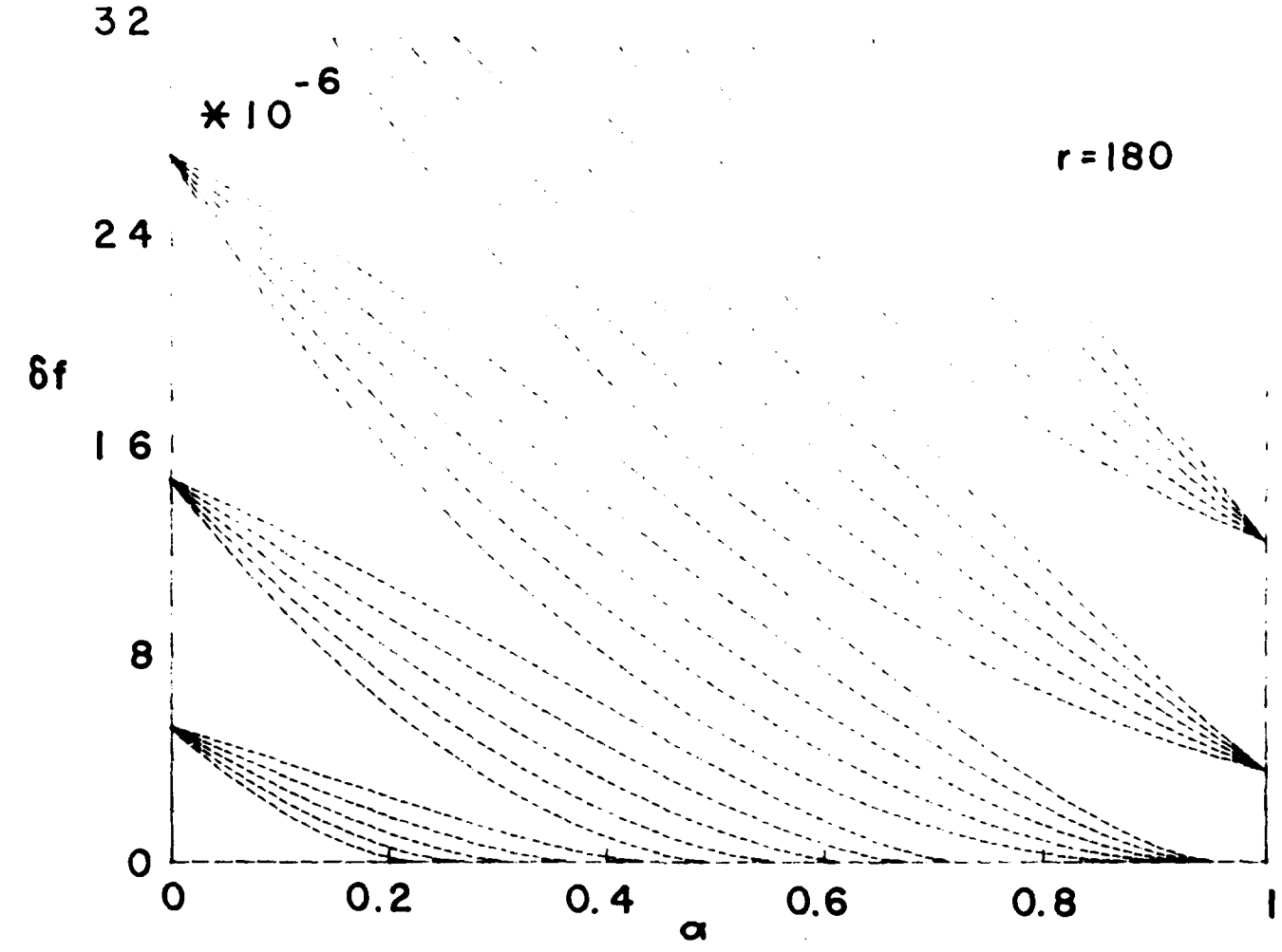

Figure 27. Petal plot of δf vs. α Δθ=2'(2')10'.

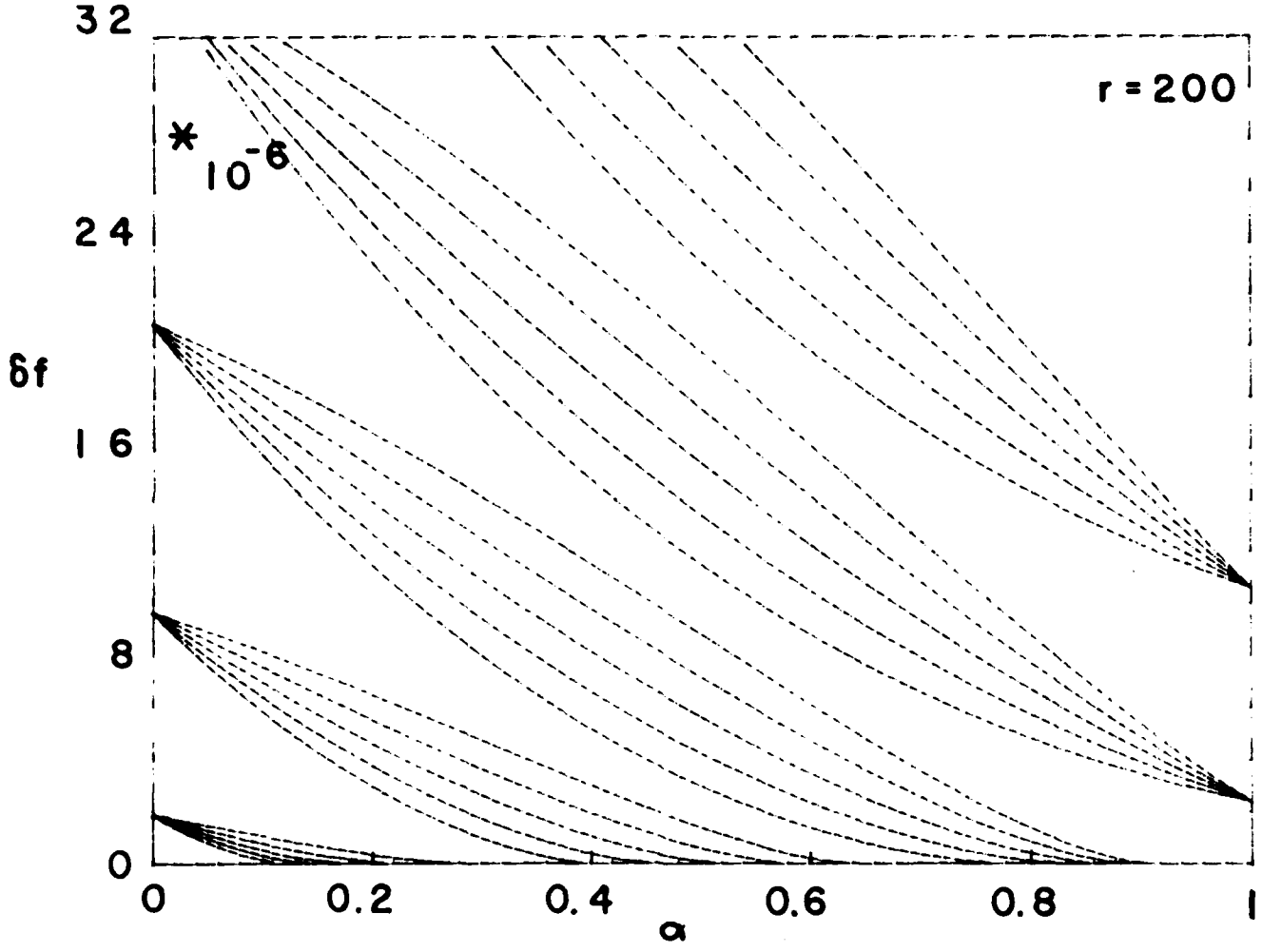

Figure 28. Petal plot of δf vs. α $\Delta\theta = 1'(2')9'$.

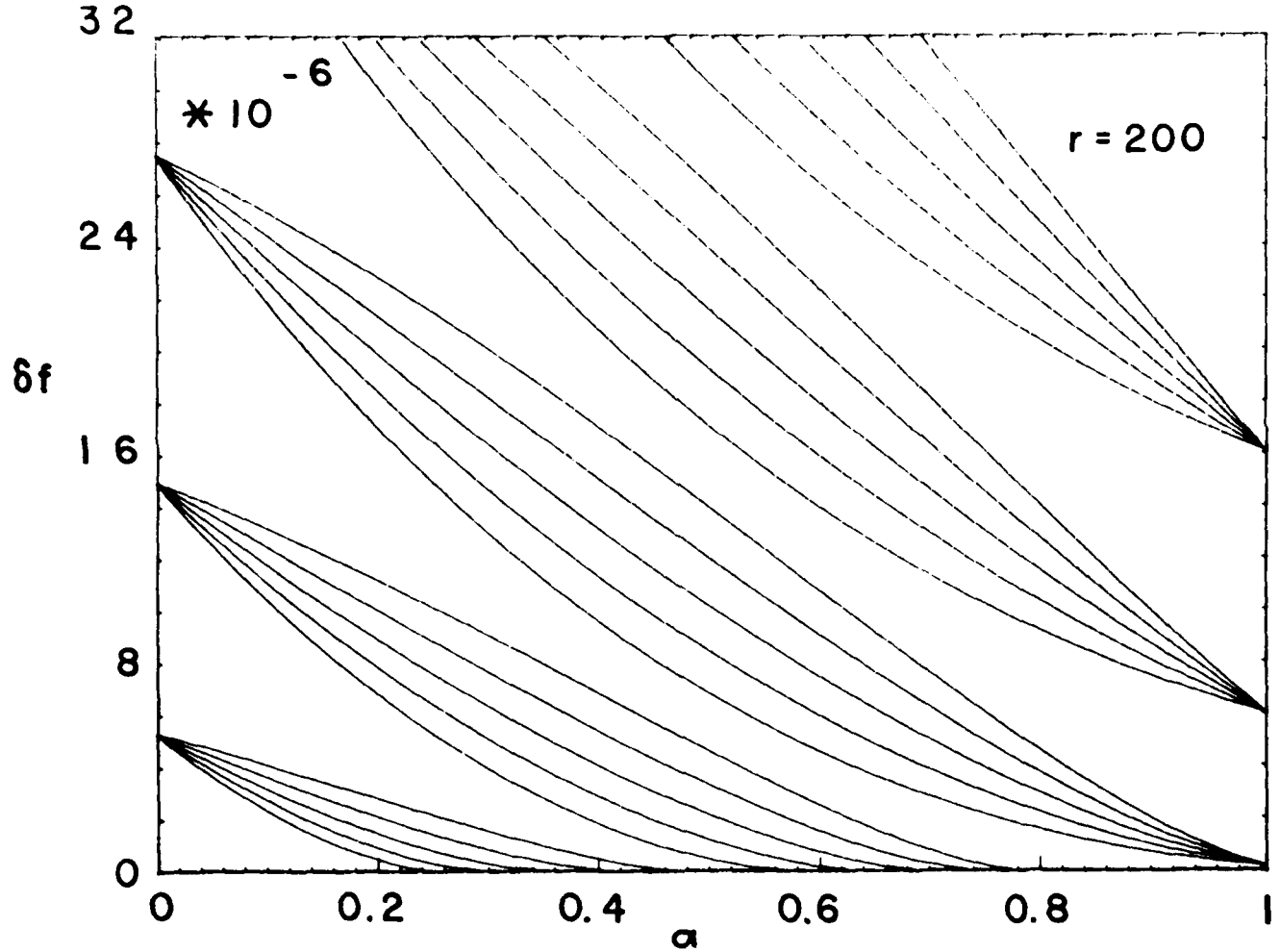

Figure 29. Petal plot of δf vs. α $\Delta\theta = 2'(2')10'$.

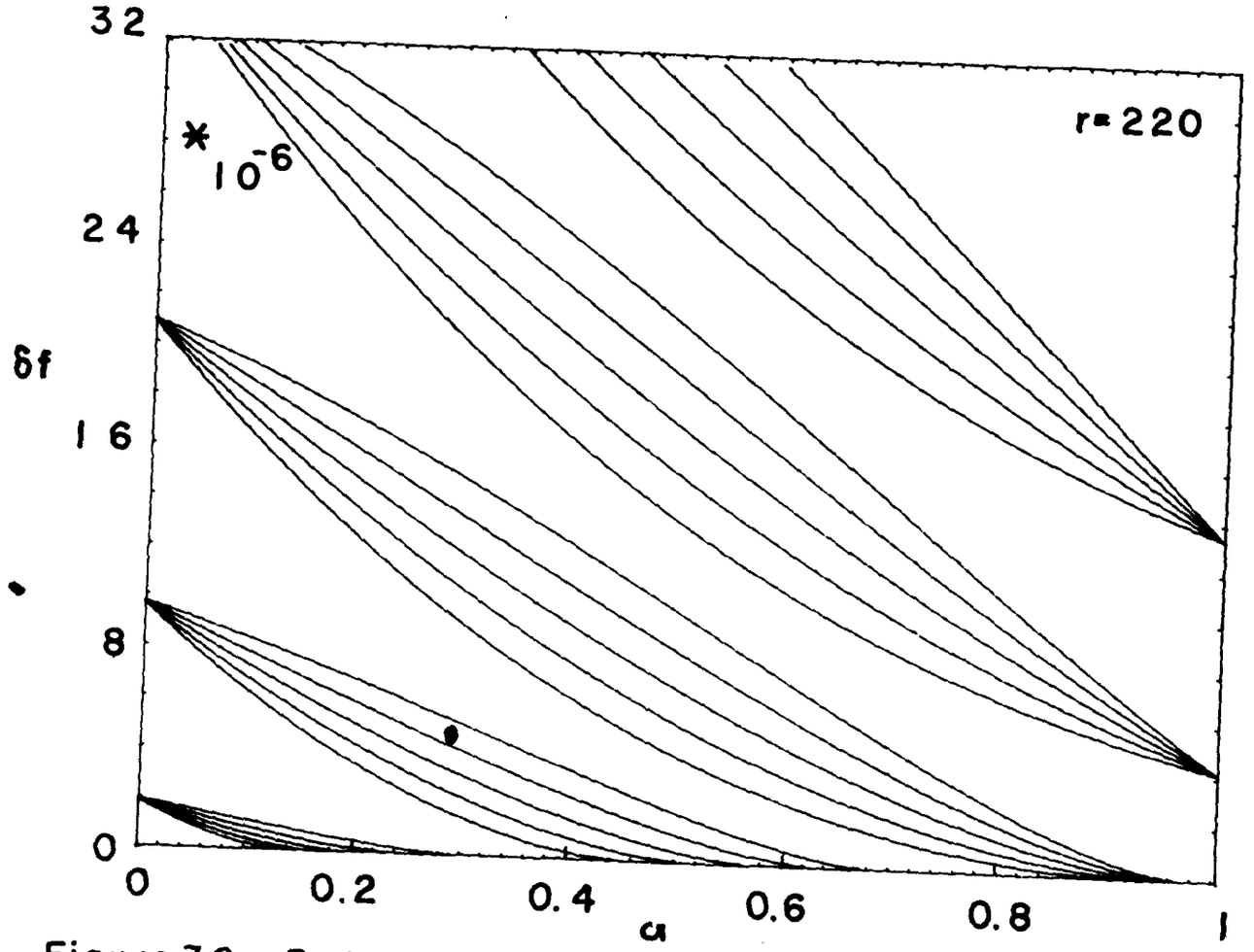

Figure 30. Petal plot of δf vs. α Δθ = 1'(2')9'.

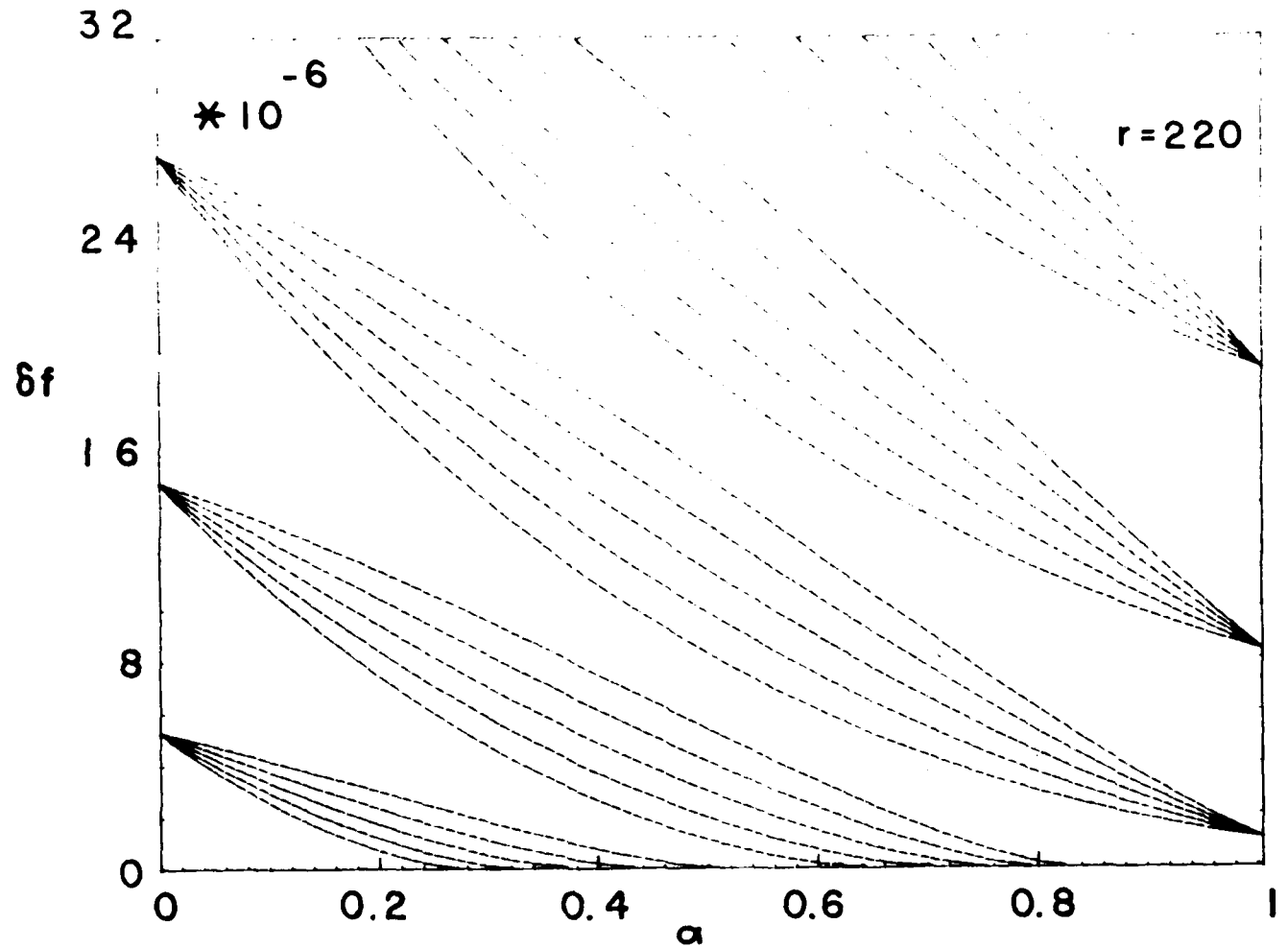

Figure 31 . Petal plot of δf vs. α Δθ = 2'(2')10'.

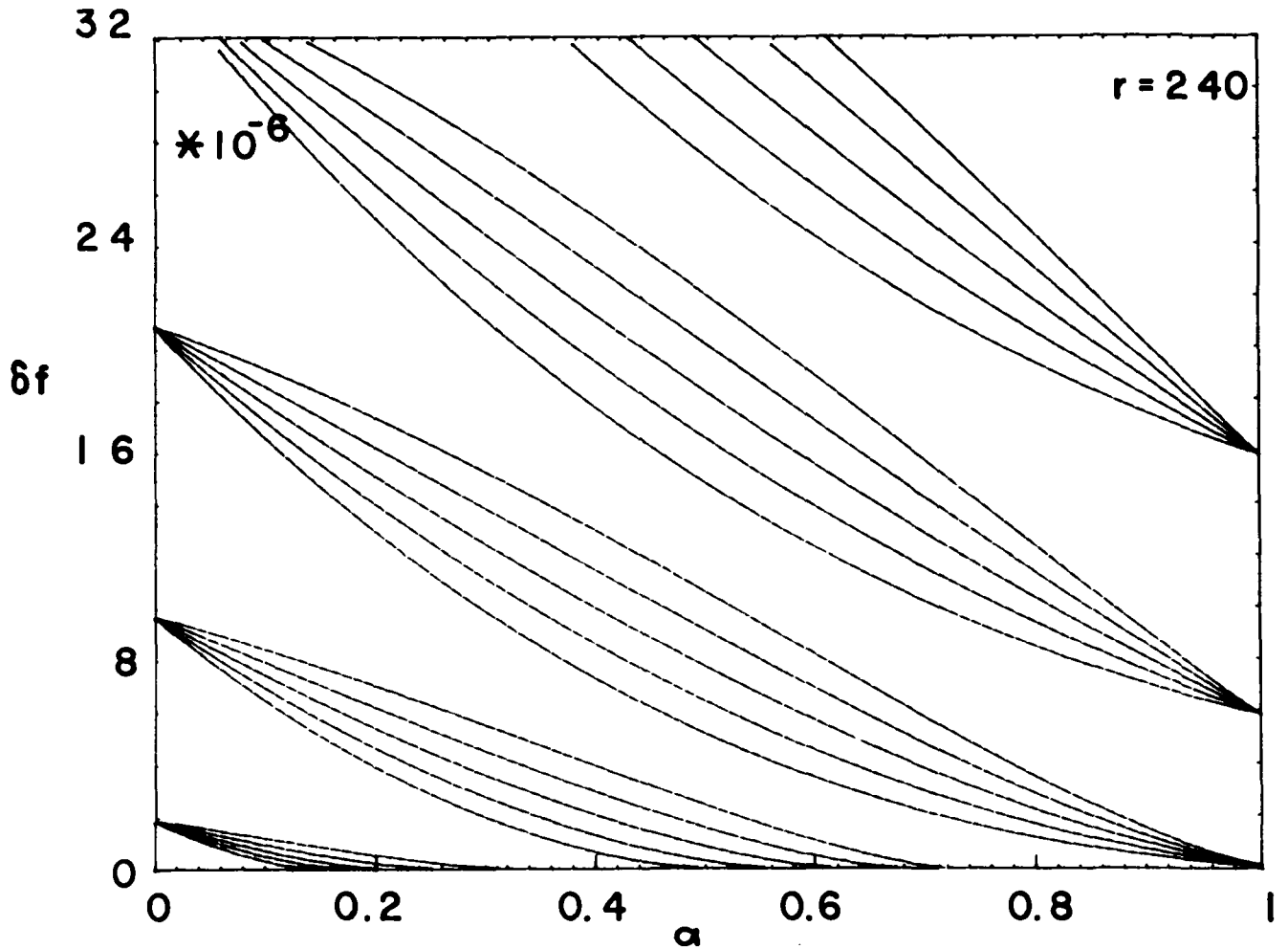

Figure 32. Petal plot of δf vs. α $\Delta\theta = 1'(2')9'$.

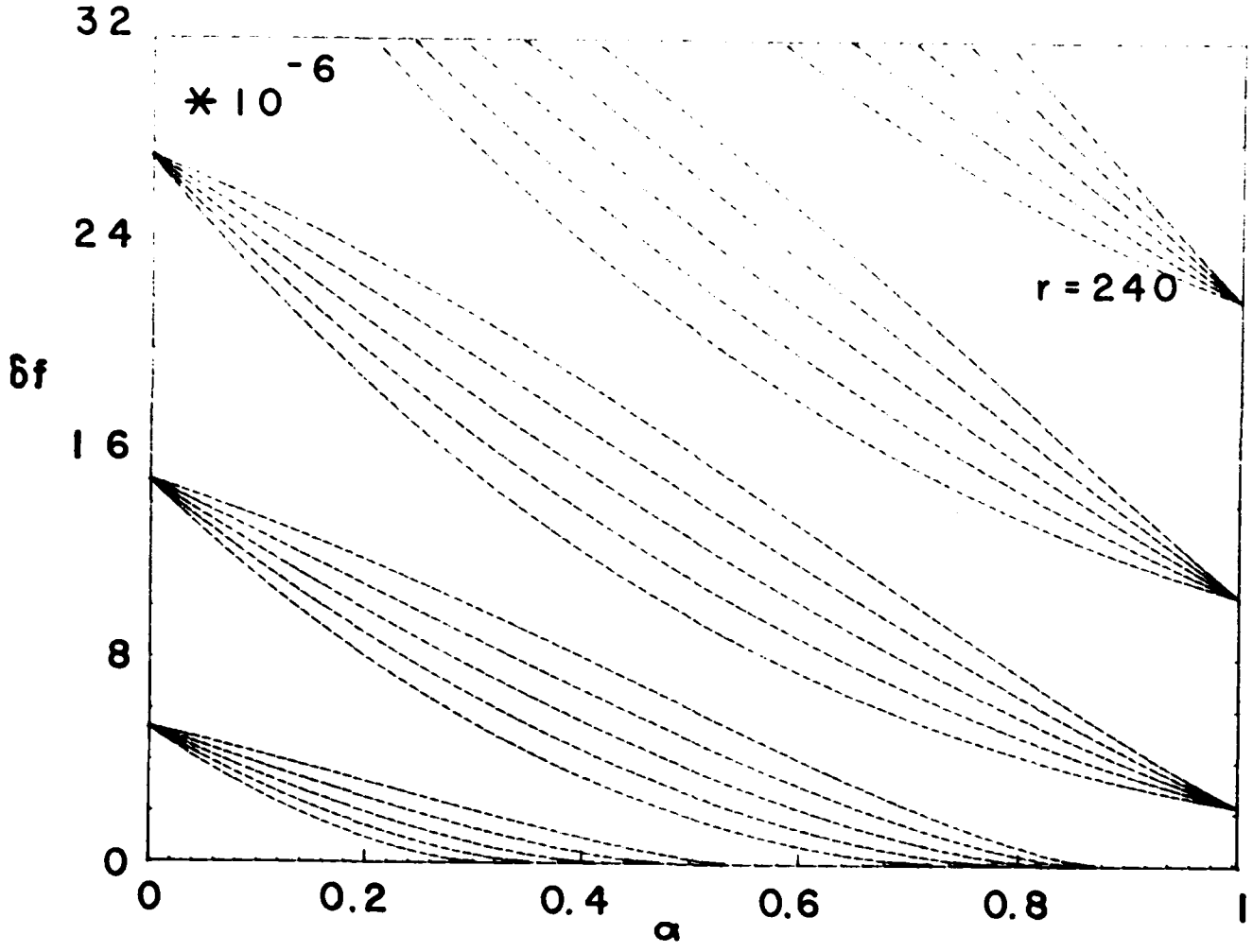

Figure 33. Petal plot of δf vs. α Δθ = 2'(2')10'.

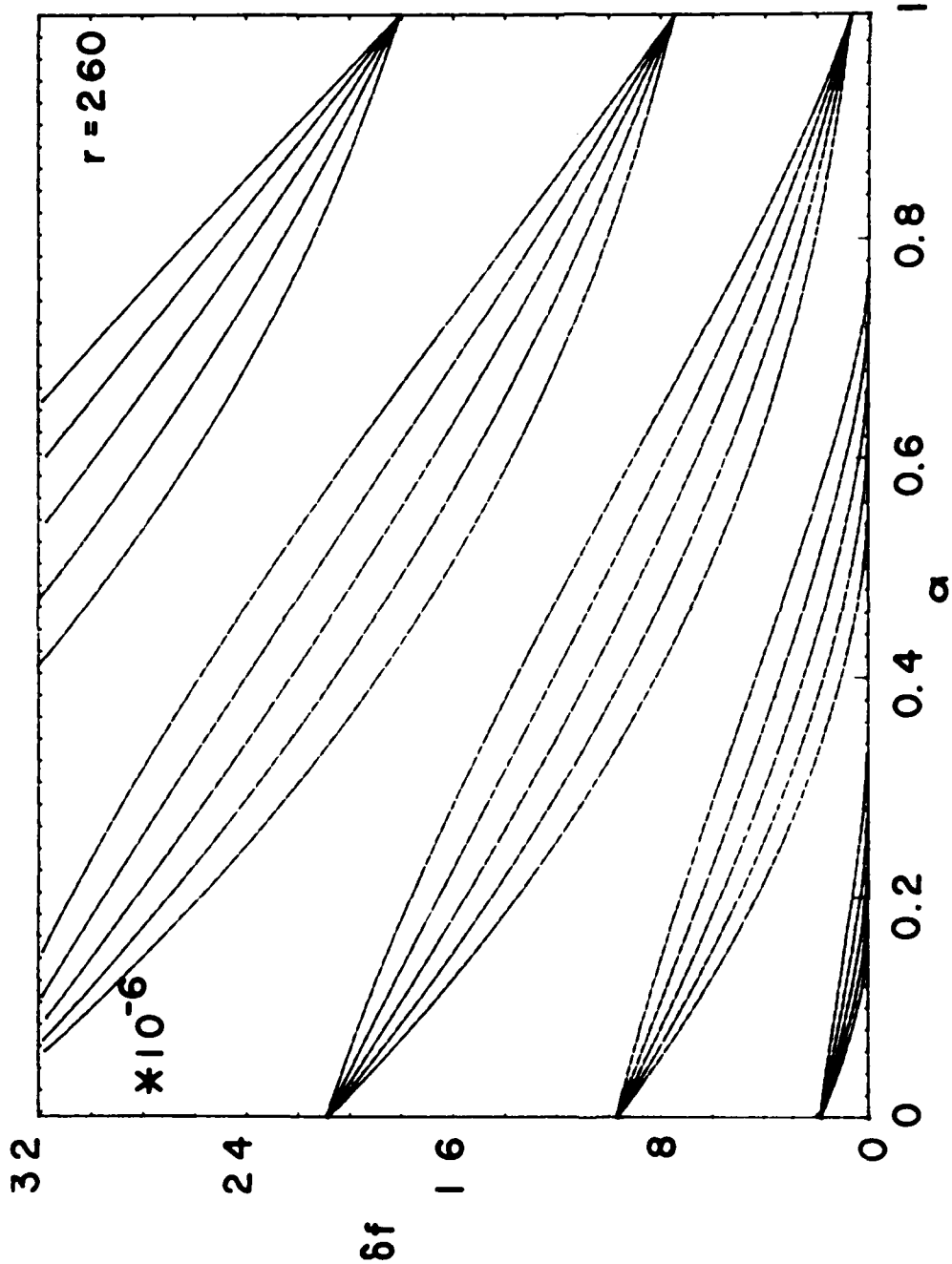

Figure 34. Petal plot of δf vs. α $\Delta\theta = l'(2')g'$.

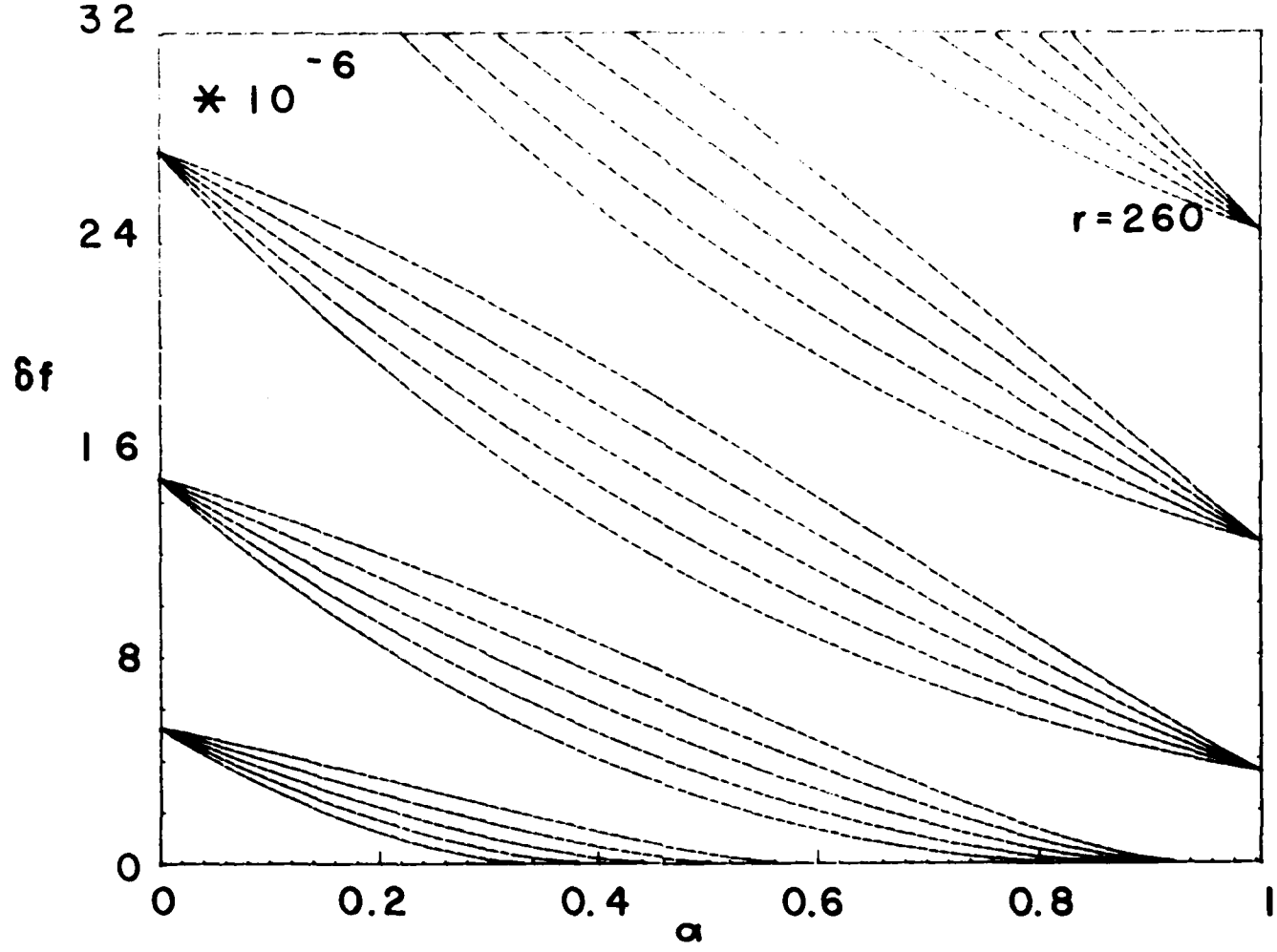

Figure 35. Petal plot of δf vs. α Δθ = 2'(2')10'.

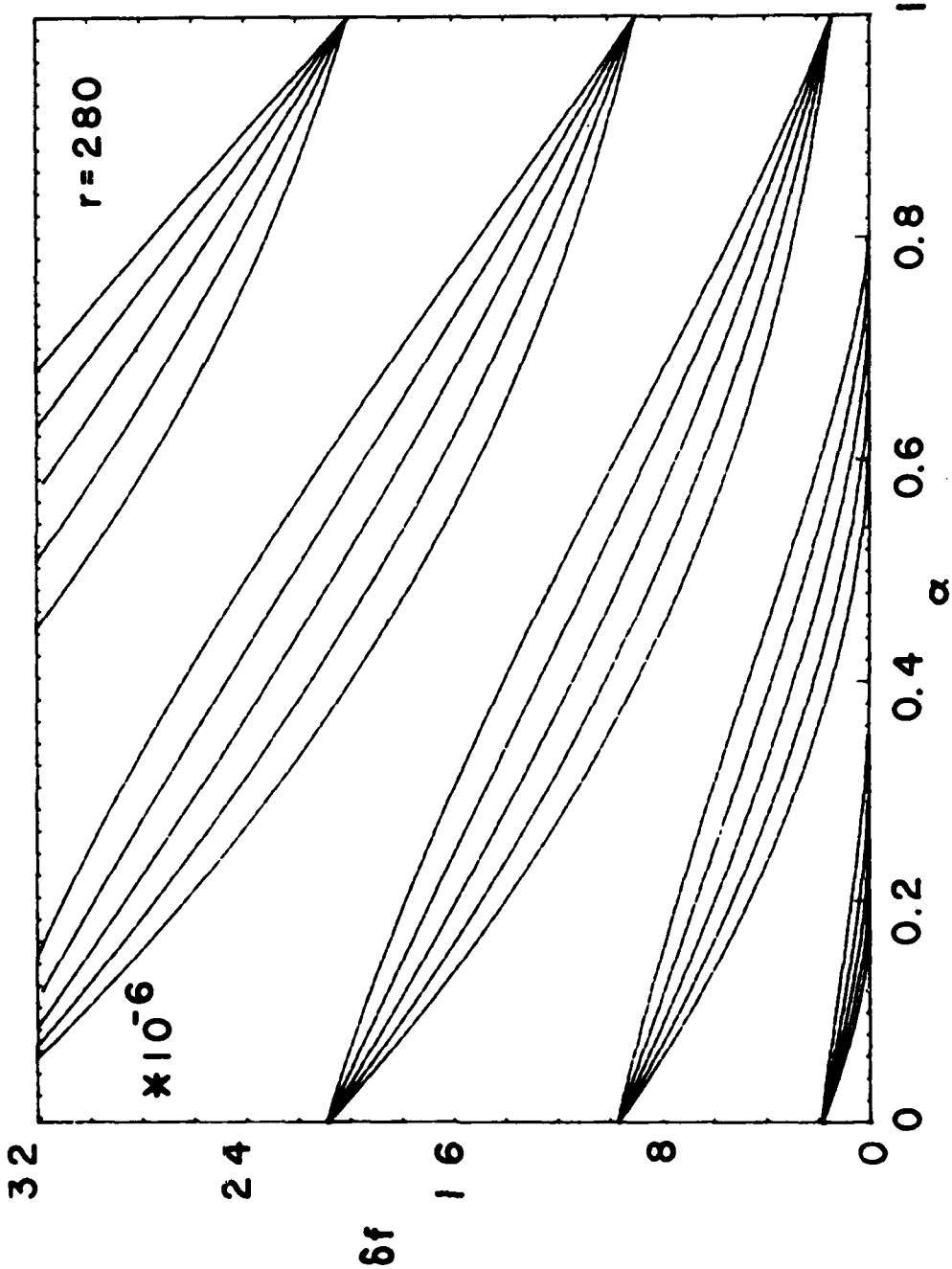

Figure 36. Petal plot of δf vs. α $\Delta\theta = 1'(2')9'$.

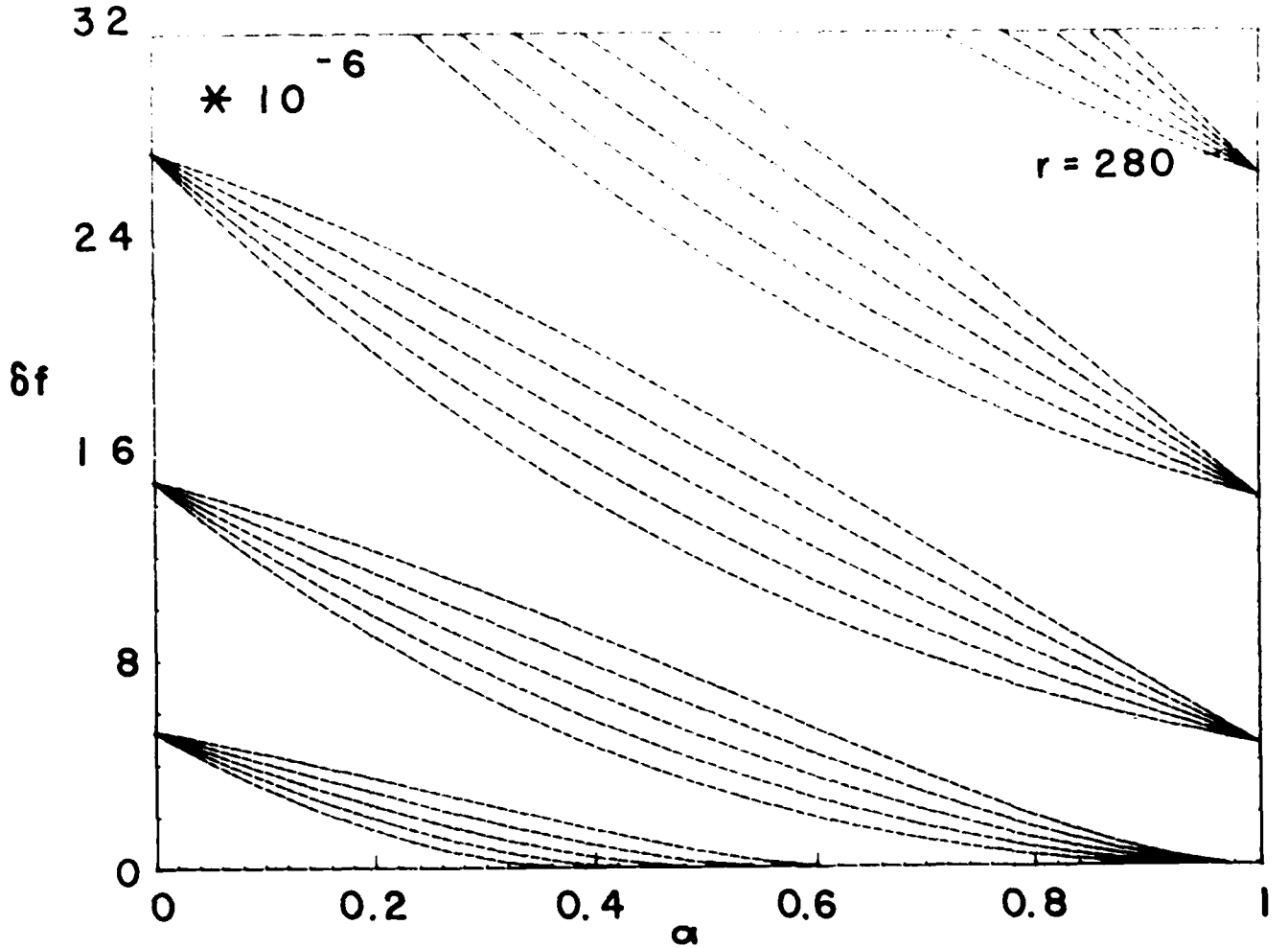

Figure37 . Petal plot of δf vs. α Δθ=2'(2')10'.

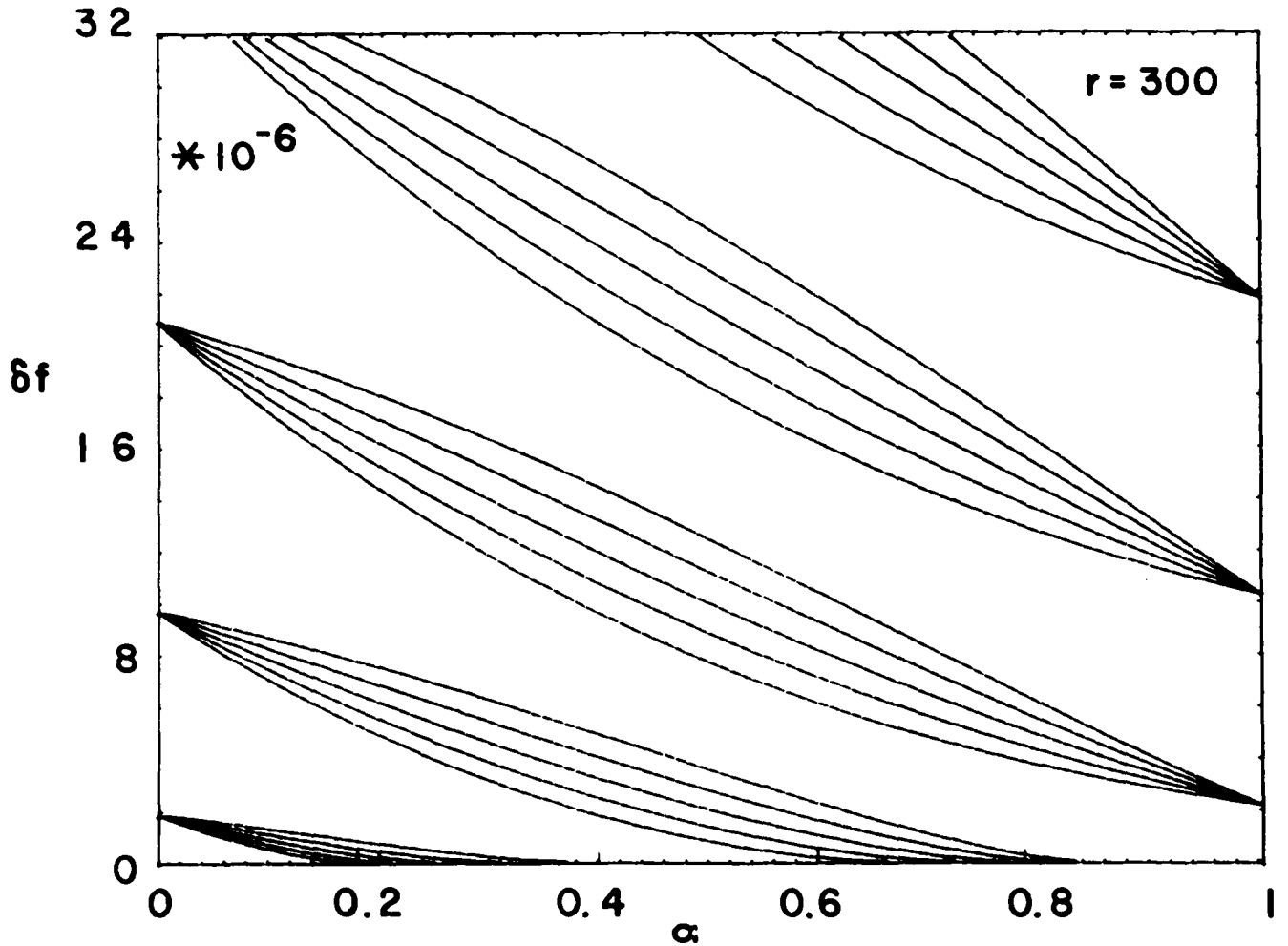

Figure 38. Petal plot of δf vs. α $\Delta\theta = 1'(2')\,9'$.

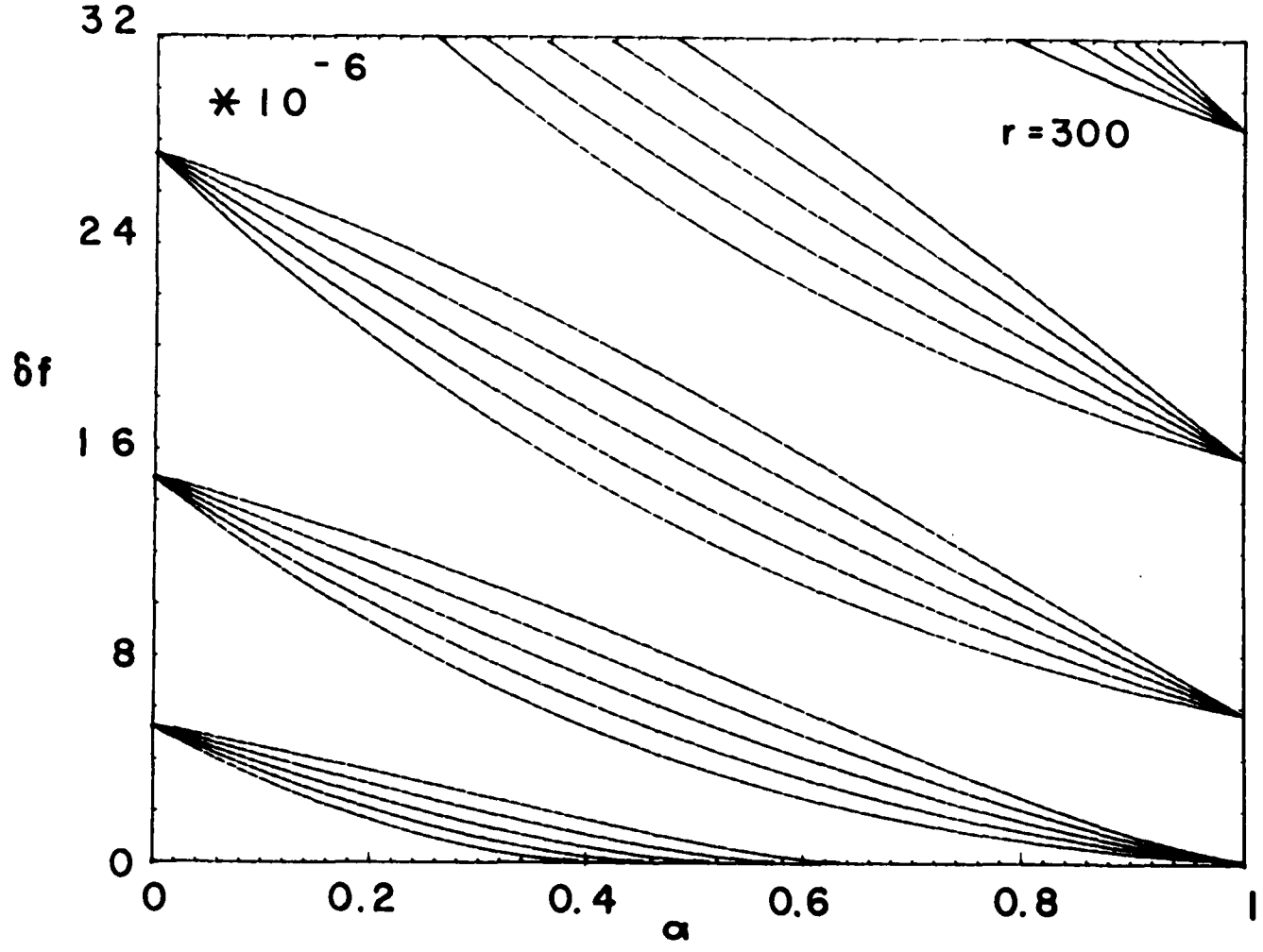

Figure 39. Petal plot of δf vs. α Δθ = 2'(2')10'.

REFERENCES*

1. N. R. Malik, "Linearizing Frequency Temperature Characteristics of Quartz Crystals by Network Synthesis," Master's Thesis, Graduate Department of Electrical Engineering, State University of Iowa, August 1960.

2. G. R. Hykes and D. E. Newell, "A Temperature-Compensated Frequency Standard," Proc. 15th AFCS, May 1961, pp. 297-317.

3. D. E. Newell, H. Hinnah, G. K. Bistline, Jr., and J. K. Reighter, "Crystal Units with Improved Temperature Characteristics," McCoy Electronics Co., Mt. Holly Springs, Pa., and The Bendix Corp., Davenport, Iowa. Final Report, Contract DA36-039 SC-90820, 1 July 1962 to 31 March 1964. US Army Electronics Command, Fort Monmouth, NJ.

4. D. E. Newell and R. H. Bangert, "Temperature Compensation of Quartz Crystal Oscillators," Proc 17th AFCS, May 1963, pp. 491-507.

5. D. E. Newell and R. H. Bangert, "Frequency Temperature Compensation Techniques for Quartz Crystal Oscillators," The Bendix Corp., Davenport, Iowa. Final Report, Contract DA36-039 SC-90782, 1 July 1962 to 30 June 1963; Interim Report, 6th Quarterly, Contract DA36-039 AMC-02282(E), 1 July 1963 to 31 December 1964. US Army Electronics Command, Fort Monmouth, NJ.

6. D. E. Newell, H. Hinnah, and R. Bangert, "Advances in Crystal Oscillator and Resonator Compensation," Proc. 18th AFCS, May 1964, pp. 487-534.

7. C. D. Dominguez, "Design and Development of Frequency Temperature Compensated Quartz Crystal Oscillator O-1227( )/U," The Bendix Corp., Davenport, Iowa. Final Report, Contract DA28-043 AMC-00042(E), 1 April 1964 to 30 September 1965. US Army Electronics Command, Fort Monmouth, NJ. AD#634520.

8. A. E. Anderson, M. E. Frerking, and G. R. Hykes, "Temperature Compensated Quartz Crystal Units," Collins Radio Co., Cedar Rapids, Iowa. Interim Report, Contract DA28-043 AMC-00210(E), 1 July 1964 to 1 April 1965. US Army Electronics Command, Fort Monmouth, NJ.

9. R. H. Bangert, H. D. Hinnah, and D. E. Newell, "Recent Developments in Crystal Oscillator Temperature Compensation," Proc. 19th AFCS, April 1965, pp. 617-641.

10. C. D. Dominguez and I. E. Hardt, "Frequency Temperature Compensation Techniques for Quartz Crystal Oscillators," The Bendix Corp., Davenport, Iowa. Final Report, Contract DA36-039 AMC-02282(E), 1 March 1965 to to 1 May, 1967. US Army Electronics Command, Fort Monmouth, NJ. AD#821964.

---

*AFCS: Annual Frequency Control Symposium, US Army Electronics Command, Fort Monmouth, NJ 07703

11. S. Schodowski, "Temperature Performance Measurements for Temperature-Compensated Quartz Oscillators," Technical Report ECOM-2896, US Army Electronics Command, Fort Monmouth, NJ, October 1967, 24 pp. AD#664157.

12. E. A. Roberts, "Temperature Compensation of AT Cut Crystals by Thermally Controlled Non-Linear Reactances," Proc. 22nd AFCS, April 1968, pp. 325-339.

13. P. G. Vovelle, "Recent Improvements to TCXO," Proc. 22nd AFCS, April 1968, pp. 311-324.

14. D. E. Newell and H. Hinnah, "Automatic Compensation Equipment for TCXO's," Proc. 22nd AFCS, April 1968, pp. 298-310.

15. H. A. Batdorf, "Temperature-Compensated Crystal-Controlled Oscillators Operating from 800 kHz to 1500 kHz," Proc. 23rd AFCS, May 1968, pp. 192-197.

16. D. E. Newell and H. Hinnah, "A Report on TCXO's and Segmented Compensation," Proc. 23rd AFCS, May 1969, pp. 187-191.

17. S. Schodowski, "A New Approach to a High Stability Temperature Compensated Crystal Oscillator," Proc. 24th AFCS, April 1970, pp. 200-208; Technical Report ECOM-3359, US Army Electronics Command, Fort Monmouth, NJ, November 1970.

18. P. C. Duckett, R. J. Peduto, and G. V. Chizak, "Temperature Compensated Crystal Oscillators," Proc. 24th AFCS, April 1970, pp. 191-199.

19. D. E. Newell and H. Hinnah, "Frequency Temperature Compensation Techniques for Quartz Crystal Oscillators," CTS Knights, Inc., Sandwich, Ill. Final Report, Contract DAAB07-67-C-0433, US Army Electronics Command, Fort Monmouth, NJ, February 1971.

20. S. Schodowski, "Design of a High Stability Voltage Controlled Crystal Oscillator," Technical Report ECOM-3532, US Army Electronics Command, Fort Monmouth, NJ, February 1972, 29 pp.

21. G. E. Buroker and M. E. Frerking, "A Digitally Compensated TCXO," Proc. 27th AFCS, June 1973, pp. 191-198.

22. D. L. Thomann, "A Microcircuit Temperature Compensated Crystal Oscillator (MCTCXO)," Proc. 28th AFCS, May 1974, pp. 214-220.

23. S. Fujii and H. Uchida, "An Analysis of Frequency Stability for TCXO," Proc. 29th AFCS, May 1975, pp. 294-299.

24. A. Mroch and G. Hykes, "High Stability Temperature Compensated Crystal Oscillator Study," Collins Radio, Cedar Rapids, Iowa 52406. Final Report, Contract DAAB07-C-0137, 28 February 1975 to 29 February 1976. US Army Electronics Command, Fort Monmouth, NJ.

25. A. B. Mroch and G. R. Hykes, "A Miniature High Stability TCXO Using Digital Compensation," Proc 30th AFCS, June 1976, pp. 292-300.

26. T. Yamada and N. Niizeki, "A New Formulation of Piezoelectric Plate Thickness Vibration," Rev. Elec. Comm. Lab. NTT (Tokyo), Vol. 19, No. 5-6, May-June 1971, pp. 705-713.

27. M. Onoe, H. F. Tiersten, and A. H. Meitzler, "Shift in the Location of Resonant Frequencies Caused by Large Electromechanical Coupling in Thickness-Mode Resonators," J. Acoust. Soc. Am., Vol. 35, January 1963, pp. 36-42.

28. A. Ballato and T. J. Lukaszek, "Mass Effects on Crystal Resonators with Arbitrary Piezo-Coupling," Proc. 27th AFCS, June 1973, pp. 20-29.

29. A. Ballato and T. Lukaszek, "Mass-Loading of Thickness-Excited Crystal Resonators Having Arbitrary Piezo-Coupling," IEEE Trans. Sonics Ultrason., Vol. SU-21, No. 4, October 1974, pp. 269-274.

30. A. Ballato and T. Lukaszek, "Mass-Loading Effects on Crystal Resonators Excited by Thickness Electric Fields," Technical Report ECOM-4270, US Army Electronics Command, Fort Monmouth, NJ, October 1974, 80 pp.

31. A. Ballato, "The Effect of Load Capacitors on the Frequency of Quartz Crystals," Technical Report ECOM-2617, US Army Electronics Command, Fort Monmouth, NJ, June 1965, 31 pp.

32. A. Ballato, "*Doubly Rotated Thickness* Mode Plate Vibrators," in Physical Acoustics (W. P. Mason and R. N. Thurston, eds.), Vol. 13, 1977, Academic Press, in press.

33. R. Bechmann, A. D. Ballato, and T. J. Lukaszek, "Higher-order Temperature Coefficients of the Elastic Stiffnesses and Compliances of Alpha-Quartz," Proc. IRE, Vol. 50, No. 8, August 1962, pp. 1812-1822, and Vol. 50, No. 12, December 1962, p. 2451; USAELRDL Technical Report 2261, US Army Electronics R & D Lab., Fort Monmouth, NJ, September 1963.

34. A. Ballato and G. J. Iafrate, "The Angular Dependence of Piezoelectric Plate Frequencies and Their Temperature Coefficients," Proc. 30th AFCS, June, 1976, pp. 141-156.

35. "Standards on Piezoelectric Crystals, 1949." Proc. IRE, Vol. 37, No. 12, December 1949, pp. 1378-1395. (IEEE Standard No. 176.)

36. R. Bechmann, "Dickenschwingungen piezoelektrisch erregter Kristallplatten," Hochfrequenztechn. u. Elektroak., Vol. 56, 1940, pp. 14-21.

37. R. Bechmann, "Influence of the Order of Overtone on the Temperature Coefficient of Frequency of AT-type Quartz Resonators," Proc. IRE, Vol. 43, No. 11, Nov. 1955, pp. 1667-1668.

38. W. G. Cady, Piezoelectricity, McGraw-Hill, NY, 1946, and Dover, NY, 1964, p. 314.

39. A. Ballato, "Normalized Frequencies and Deviations as Function of Coupling, Mass-Loading and Harmonic: Numerical Results for Thickness Excitation," Technical Report ECOM-4354, US Army Electronics Command, Fort Monmouth, NJ, September 1975, 164 pp.

40. R. Bechmann, "Frequency-Temperature-Angle Characteristics of AT-type Resonators Made of Natural and Synthetic Quartz," Proc. IRE, Vol. 44, No. 11, November 1956, pp. 1600-1607.

41. R. Bechmann, "Frequency-Temperature-Angle Characteristics of AT- and BT-type Quartz Oscillators in an Extended Temperature Range," Proc. IRE, Vol. 48, No. 8, August 1960, p. 1494.

42. A. Ballato, "Effect of Second Rotation on Frequency-Temperature Characteristics of AT-Cut Crystals," Technical Report ECOM-4424, US Army Electronics Command, Fort Monmouth, NJ, August 1976, 10 pp.

43. A. Ballato and T. Lukaszek, "Higher-Order Temperature Coefficients of Frequency of Mass-Loaded Piezoelectric Crystal Plates," Proc. 29th AFCS, May 1975, pp. 10-25.

44. A. Ballato and T. Lukaszek, "Frequency-Temperature Coefficients of Mass-Loaded Plate Vibrators," Technical Report ECOM-4356, US Army Electronics Command, Fort Monmouth, NJ, September 1975, 49 pp.

45. A. Ballato, "Alteration of Temperature Coefficients in Mass-Loaded Crystal Vibrators," Technical Report ECOM-4360, US Army Electronics Command, Fort Monmouth, NJ, October 1975, 9 pp.

46. A. Ballato, "Apparent Orientation Shifts of Mass-Loaded Plate Vibrators," Proc. IEEE, Vol. 64, No. 9, September 1976, pp. 1449-1450.

47. M. Onoe, "Relationship between Temperature Behavior of Resonant and Antiresonant Frequencies and Electromechanical Coupling Factors of Piezoelectric Resonator," Proc. IEEE, Vol. 57, No. 4, April 1969, pp. [illegible]

48. [illegible] resonators," IEEE Trans. Sonics Ultrason., [illegible] 1974, pp. 220-237.

[illegible] [illegible]aszek, and A. Ballato, "Practical Consequences [illegible] in Crystal Resonators," Proc. 21st AFCS, [illegible] Technical Report ECOM-2847, US Army Electronics [illegible] June 1967, 21 pp.

[illegible] [illegible]schwingungen piezoelectrischer Kristall- [illegible] Übertragung, Vol. 6, September 1952, pp. [illegible]